A&A, 689, A148 (2024)
https://doi.org/10.1051/0004-6361/202450584


Astronomy & Astrophysics

# The VISTA Variables in the Vía Láctea eXtended (VVVX) ESO public survey: Completion of the observations and legacy*

R. K. Saito[1], M. Hempel[2,3], J. Alonso-García[4,5], P. W. Lucas[6], D. Minniti[2,7,1], S. Alonso[8], L. Baravalle[9,10], J. Borissova[11,12], C. Caceres[2], A. N. Chené[13], N. J. G. Cross[14], F. Duplancic[8], E. R. Garro[15], M. Gómez[2], V. D. Ivanov[16], R. Kurtev[11,12], A. Luna[17], D. Majaess[18], M. G. Navarro[19], J. B. Pullen[2], M. Rejkuba[16], J. L. Sanders[20], L. C. Smith[21], P. H. C. Albino[1], M. V. Alonso[9,10], E. B. Amôres[22], R. Angeloni[23], J. I. Arias[24], M. Arnaboldi[16], B. Barbuy[25], A. Bayo[16], J. C. Beamin[2,26], L. R. Bedin[27], A. Bellini[28], R. A. Benjamin[29], E. Bica[30], C. J. Bonatto[30], E. Botan[31], V. F. Braga[19], D. A. Brown[32], J. B. Cabral[9,33], D. Camargo[34], A. Caratti o Garatti[17], J. A. Carballo-Bello[35], M. Catelan[36,5,37], C. Chavero[10,38], M. A. Chijani[2], J. J. Clariá[10,38], G. V. Coldwell[8], C. Contreras Peña[39], R. Contreras Ramos[36,5], J. M. Corral-Santana[15], C. C. Cortés[40], M. Cortés-Contreras[41], P. Cruz[42], I. V. Daza-Perilla[38,9,43], V. P. Debattista[44], B. Dias[2], L. Donoso[45], R. D'Souza[7], J. P. Emerson[46], S. Federle[15,2], V. Fermiano[1], J. Fernandez[8], J. G. Fernández-Trincado[47], T. Ferreira[48], C. E. Ferreira Lopes[49,5], V. Firpo[23], C. Flores-Quintana[2,5], L. Fraga[50], D. Froebrich[51], D. Galdeano[8], I. Gavignaud[2], D. Geisler[52,53,24], O. E. Gerhard[54], W. Gieren[52], O. A. Gonzalez[55], L. V. Gramajo[10,38], F. Gran[56], P. M. Granitto[57], M. Griggio[27,58,28], Z. Guo[11,12], S. Gurovich[9,59], M. Hilker[16], H. R. A. Jones[6], R. Kammers[1], M. A. Kuhn[6], M. S .N. Kumar[60], R. Kundu[61,62], M. Lares[9], M. Libralato[27], E. Lima[63], T. J. Maccarone[64], P. Marchant Cortés[24], E. L. Martin[65,66], N. Masetti[67,2], N. Matsunaga[68], F. Mauro[47], I. McDonald[69], A. Mejías[70], V. Mesa[53,71,72], F. P. Milla-Castro[24], J. H. Minniti[73], C. Moni Bidin[47], K. Montenegro[74], C. Morris[6], V. Motta[11], F. Navarete[75], C. Navarro Molina[76], F. Nikzat[36,5], J. L. Nilo Castellón[53,24], C. Obasi[47,77], M. Ortigoza-Urdaneta[78], T. Palma[10], C. Parisi[10,9], K. Pena Ramírez[79], L. Pereyra[9], N. Perez[8], I. Petralia[2], A. Pichel[80], G. Pignata[35], S. Ramírez Alegría[4], A. F. Rojas[36,81,4], D. Rojas[2], A. Roman-Lopes[24], A. C. Rovero[80], S. Saroon[2], E. O. Schmidt[10,9], A. C. Schröder[82], M. Schultheis[56], M. A. Sgró[10], E. Solano[42], M. Soto[49], B. Stecklum[83], D. Steeghs[84], M. Tamura[68,85,86], P. Tissera[36,37], A. A. R. Valcarce[87], C. A. Valotto[9,10], S. Vasquez[88], C. Villalon[9,10], S. Villanova[52], F. Vivanco Cádiz[2], R. Zelada Bacigalupo[89], A. Zijlstra[69,90], and M. Zoccali[36,5]

*(Affiliations can be found after the references)*

Received 2 May 2024 / Accepted 14 June 2024

**ABSTRACT**

*Context.* The ESO public survey VISTA Variables in the Vía Láctea (VVV) surveyed the inner Galactic bulge and the adjacent southern Galactic disk from 2009–2015. Upon its conclusion, the complementary VVV eXtended (VVVX) survey has expanded both the temporal as well as spatial coverage of the original VVV area, widening it from 562 to 1700 sq. deg., as well as providing additional epochs in $JHK_s$ filters from 2016–2023.

*Aims.* With the completion of VVVX observations during the first semester of 2023, we present here the observing strategy, a description of data quality and access, and the legacy of VVVX.

*Methods.* VVVX took ~2000 h, covering about 4% of the sky in the bulge and southern disk. VVVX covered most of the gaps left between the VVV and the VISTA Hemisphere Survey (VHS) areas and extended the VVV time baseline in the obscured regions affected by high extinction and hence hidden from optical observations.

*Results.* VVVX provides a deep $JHK_s$ catalogue of $\gtrsim 1.5 \times 10^9$ point sources, as well as a $K_s$ band catalogue of $\sim 10^7$ variable sources. Within the existing VVV area, we produced a 5*D* map of the surveyed region by combining positions, distances, and proper motions of well-understood distance indicators such as red clump stars, RR Lyrae, and Cepheid variables.

*Conclusions.* In March 2023 we successfully finished the VVVX survey observations that started in 2016, an accomplishment for ESO Paranal Observatory upon 4200 h of observations for VVV+VVVX. The VVV+VVVX catalogues complement those from the *Gaia* mission at low Galactic latitudes and provide spectroscopic targets for the forthcoming ESO high-multiplex spectrographs MOONS and 4MOST.

**Key words.** surveys – Galaxy: bulge – Galaxy: disk – Galaxy: stellar content – infrared: stars

* Based on observations taken within the ESO VISTA Public Survey VVV and VVVX, Programmes ID 179.B-2002 and 198.B-2004, respectively.

## 1. Introduction

Despite large-scale optical surveys over many decades, the internal structure of the inner regions of the Milky Way (MW) and the details of its formation and evolution were poorly understood. The main reason is the severe and non-uniform interstellar extinction and crowding towards the MW bulge and inner disk, which complicates observations, especially at the optical wavelengths. These inner regions are the most complex of our Galaxy to study, with a mixture of stellar populations from the inner disk, bulge, and halo, which exhibit a variety of physical properties.

This situation has improved in recent years, with several projects studying the inner regions of the MW (e.g. Barbuy, Chiappini, & Gerhard 2018; Saviane et al. 2020, and references therein). The VISTA Variables in the Vía Láctea (VVV) survey (Minniti et al. 2010) was designed to resolve the 3D structure of the MW by searching, precisely parameterising, and studying the distributions of known distance indicators such as RR Lyrae, Cepheids, and red clump stars in the inner Galaxy. By using observations at near-infrared wavelengths, VVV observations minimise the problems of extinction and crowding. Among many results, the VVV data have enabled the construction of high-resolution extinction and photometric metallicity maps (e.g. Gonzalez et al. 2012, 2013), the discovery of stellar clusters (e.g. Borissova et al. 2014), and the production of 3D spatial structure maps based on red clump and RR Lyrae stars (e.g. Dékány et al. 2013; Wegg & Gerhard 2013).

In 2016, the VVV eXtended (VVVX) survey started operating. The VVVX survey was designed to ensure the long-term legacy of the VVV survey, characterising the structure and time domain properties of the inner Galaxy. The project is one of seven large public surveys (Arnaboldi et al. 2019) commissioned by the European Southern Observatory (ESO). The VVV+VVVX surveys were awarded about 4200 h of observing time over a timespan of ∼13 years at the 4-metre Visible and Infrared Survey Telescope for Astronomy (VISTA; Emerson, McPherson, & Sutherland 2006) telescope at ESO Paranal Observatory, and were finally completed in March 2023, before the VISTA InfraRed CAMera (VIRCAM; Dalton et al. 2006; Emerson & Sutherland 2010) instrument was decommissioned from the VISTA telescope. Both surveys combined cover the Galactic bulge, as well as the adjacent disk towards the Galactic quadrants I and IV.

The VVV survey pioneered the discovery of variable stars, transients, and a select number of new clusters across a significant region around the Galactic centre and plane. VVVX bridges the gap between VVV findings and other surveys, extending into obscured regions. This aids in estimating survey completeness and mapping distributions of various tracers from the halo to the Galactic centre. The VVVX survey was designed to connect the VVV survey area with the VISTA Hemisphere Survey (VHS; McMahon et al. 2013) and the UKIDSS Galactic Plane Survey (Lucas et al. 2008). VVVX overlaps with the VST Photometric H$\alpha$ Survey (VPHAS+; Drew et al. 2014) and the DECam Plane Survey (DECaPS; Schlafly et al. 2018), providing complementary near-IR imaging for those regions (see Fig. 1) as well as variability information. In addition, by re-observing the area of the original VVV, VVVX extends both the time baseline as well as reaches fainter flux limits, complementing other public optical and far-IR surveys. In particular, the mapped regions are located between Galactic longitudes $l = -130$ degrees and $l = +20$ degrees, detecting $\gtrsim 1.5 \times 10^9$ point sources in an area of around 1,700 square degrees, including more than 50 known globular clusters and 1,000 open clusters. The specific goals of the VVVX survey stated in the original proposal are:

- To map the structure of the optically obscured populations in position and velocity.
- To find pulsating variable stars (RR Lyrae, Classical Cepheids, Type 2 Cepheids, Miras) as distance indicators probing the 3D structure of the inner MW.
- To physically characterise known and newly detected star clusters (open star clusters as well as globular clusters), measuring their distances, extinctions, reddenings, sizes, and estimating their metallicities and ages.
- To explore the stellar populations and variable stars of the Sagittarius dwarf galaxy located beyond the Galactic bulge.
- To find rare variable sources such as transients and WIT ('What Is This?') objects, and also to identify the near-IR counterparts of benchmark high-energy sources discovered by recent X-ray missions.
- To build a catalogue with the classification of dwarf stars beyond the peak of the luminosity function and their companions.
- To detect heretoforth unknown background galaxies and QSOs in the Galactic Zone of Avoidance (ZoA).
- To probe the Galactic structure close to the Galactic centre using near-IR microlensing.

VVVX observations provide essential input targets for spectroscopic surveys based on multiplexing spectrographs such as the SDSS-IV/V (Sloan Digital Sky Survey-IV/V; Blanton et al. 2017; Kollmeier et al. 2019), the Galactic 4MOST surveys (4-metre Multi-Object Spectroscopic Telescope; de Jong et al. 2019)[1] and MOONS Galactic survey (Multi-Object Optical and Near-infrared Spectrograph; Gonzalez et al. 2020). In addition, our database complements measurements from important current and future space missions such as the *Hubble* Space Telescope (HST), *Gaia*, *James Webb* Space Telescope (JWST), *Euclid*, and *Nancy Grace Roman* Space Telescope.

There is a variety of final products, including deep $JHK_s$ images, multi-band $JHK_s$ and multi-epoch $K_s$ band time series catalogues, and proper motions for $\gtrsim$1.5 billion sources. Moreover, VVVX catalogues millions of variable stars, extend the VVV extinction and reddening maps, and increase the completeness and source density maps, thus presenting a treasure trove for the whole astronomical community. The VVVX public database will offer the possibility to explore a wide variety of scientific objectives, from those we listed previously to new ones, including serendipitous discoveries.

Due to its larger survey area VVVX provides a more complete picture of the inner MW than its predecessor VVV: a deep bulge map to establish structure differences between the oldest and younger populations, a map of the Sagittarius dwarf from its core across the whole bulge, and a much more extended disk map that probes star formation (SF) activity, disk stellar populations, and spiral arms structure. VVVX provides a public multicolour time domain database within the optically hidden MW regions, including 3D extinction maps that trace the non-stellar baryonic matter. Additionally, the VVVX survey provides observational constraints for the present-day MW structure as presently known (e.g., thin and thick disk structure, number of spiral arms and their locations), and even more importantly, provides insights into the assembly history of the MW.

The aim of this article is to describe the VVVX survey design, observations, data processing, and final status of

[1] https://www.4most.eu/cms/science/galactic-community-surveys/

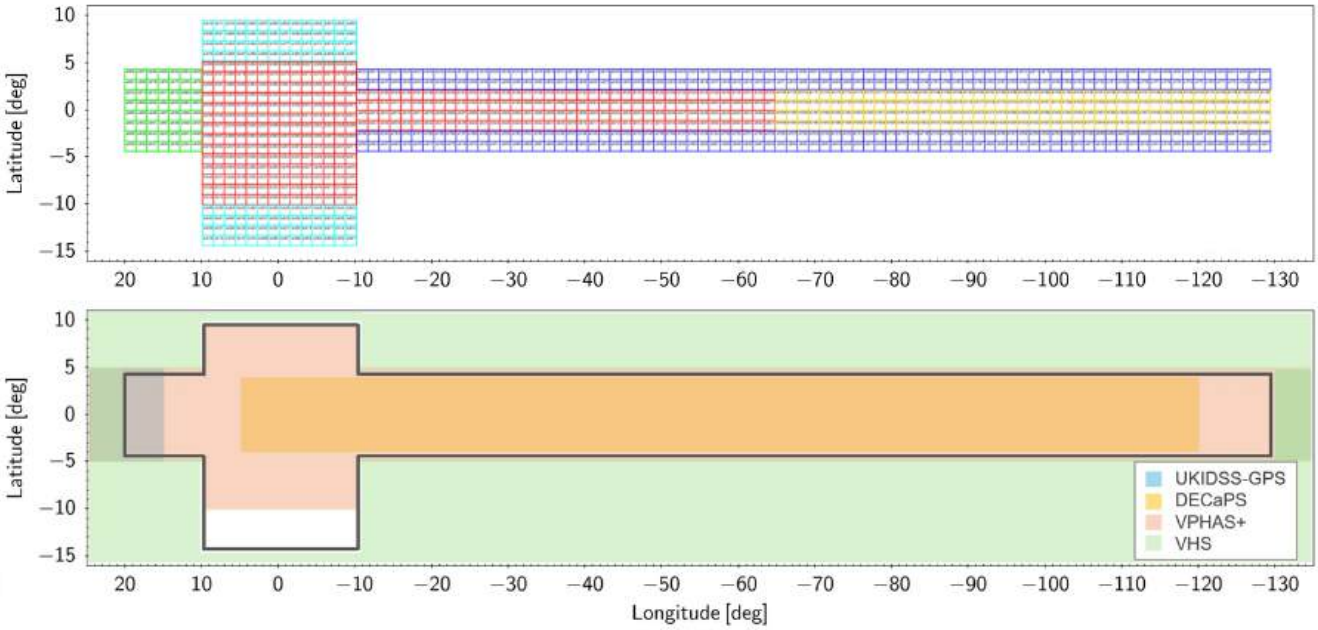


**Fig. 1.** VVV+VVVX survey coverage of the MW bulge and southern plane. Top: the surveyed area shown Galactic coordinates. Our near-IR survey covers ∼1700 sq. deg. in total, and the different regions are colour-coded according to the location, baseline, and number of observations (see Sect. 4). In red is the original VVV Bulge and VVV Disk, with observations from years 2010 and 2016 using the $ZYJHK_s$ filters, and VVVX observations between years 2016 and 2022 using the $JHK_s$ filters. Other colours mark the VVVX areas, observed with $JHK_s$ filters between years 2016 to 2022. Yellow is the Disk to Longitude +230, dark blue is the Low and High Extended Disk, green is the Disk to Longitude +20, and in light blue is the Low and High Extended Bulge. A zoomed view of the image with the tile names is presented in Appendix A. Bottom: Schematic representation of the areal coverage compared with the other selected complementary surveys mentioned in Sect. 1.

the VVVX survey, emphasising the observation strategy and describing the observed data available to the astronomical community through the VISTA Science Archive (VSA) and ESO Science Archive. We also describe some usage examples of VVVX data within the MW and beyond. In the ESO Science Archive the VVV and VVVX data are published in the data collections identified by doi.eso.org/10.18727/archive/67 and doi.eso.org/10.18727/archive/68.

## 2. Telescope and instrument

The VVVX observations were carried out with Visible and Infrared Survey Telescope for Astronomy (VISTA), an ESO telescope located at the Cerro Paranal Observatory in the Atacama Desert, northern Chile. For all VISTA photometric surveys, the VIRCAM camera was used (Dalton et al. 2006; Emerson & Sutherland 2010). VIRCAM was equipped with sixteen 2048 × 2048 science detectors, arranged in a 4 × 4 array, with a large spacing of 90% and 42.5% of the detector size along the $X$ and $Y$ axes. Each individual detector covered ∼ 694 × 694 arcsec$^2$ on the sky, with 0.″339 average pixel scale. Its filter wheel was equipped with five broad-band filters ($Z$, $Y$, $J$, $H$, and $K_s$) and two narrow-band filters centred at 0.98 and 1.18 µm. For the VVVX observations only $JHK_s$ were used. Table 1 shows the centre wavelengths of each filter.

In all VIRCAM observations, each pointing of the telescope is a so-called a pawprint, which covers 0.59 sq. deg. and provides partial, coverage of the field of view. By combining six pawprint exposures with appropriate offsets, the contiguous coverage of a field is achieved with at least two exposures on separate pixels, except at the edges. That is called a tile and covers a field of view of 1.109 × 1.475 = 1.646 sq. deg., the largest unvignetted field of view in the near-IR regime on 4-m class telescopes.

**Table 1.** VISTA filters used in the VVVX observations.

| Filter | $\lambda_{\rm eff}$(µm) | $A_X/A_V$ | $A_X/E(B-V)$ |
|---|---|---|---|
| $J$ | 1.254 | 0.280 | 0.866 |
| $H$ | 1.646 | 0.184 | 0.567 |
| $K_s$ | 2.149 | 0.118 | 0.364 |

**Notes.** The effective wavelengths for the three VISTA filters used in the VVVX observations are shown along with the relative extinction for each filter based on the Cardelli et al. (1989) extinction law (from Catelan et al. 2011).

In 2023, VIRCAM was decommissioned and will subsequently be replaced by the fibre-fed spectrograph 4MOST (de Jong et al. 2019). In fact, various 4MOST surveys will collect complementary spectroscopic data to VVV and VVVX. For details about the telescope and instrument, we refer the interested reader to Sutherland et al. (2015) and the VIRCAM instrument web-pages[2], and the VISTA/VIRCAM user manual (Ivanov et al. 2021).

## 3. Survey area

The VVV survey observed ∼562 sq deg in the MW bulge and the adjacent southern Galactic plane. The area was divided in bulge, with ∼300 sq. deg. within $-10.0° \lesssim l \lesssim +10.4°$ and $-10.3° \lesssim b \lesssim +5.1°$, hereafter called 'VVV Bulge', and ∼ 220 sq. deg. within $294.7° \lesssim l \lesssim 350°$ and $-2.25° \lesssim b \lesssim +2.25°$, hereafter 'VVV Disk' (see Fig. 1). For the VVV Disk there is a total of 38 × 4 = 152 tiles while the VVV Bulge is filled up by

[2] https://www.eso.org/sci/facilities/paranal/decommissioned/vircam.html

$14 \times 14 = 196$ tiles. The tile sides are aligned with the Galactic coordinates for coverage optimisation.

The VVVX survey expanded the area of the original VVV footprint in both Galactic longitude and latitude, with an area of ~480 deg$^2$ in the Galactic bulge plus ~1170 deg$^2$ in the inner plane (including the original VVV), from $l = -130$ deg to $l = +20$ deg (7 h <RA< 19 h). For contiguous observations of large areas, the covering process was carried out using the 'Survey Area Definition Tool' (SADT[3]), which maximises the efficiency of VISTA observations by minimising the number of tiles needed to cover a given area, providing the tile centres and the guide and active optics stars necessary for the execution of the survey Observing Blocks (OBs). The new areas – with their respective tiles – were labelled as following:

- Low extended disk (disk-low, for short): area with the lowest latitudes along the disk, located within $+230° \lesssim l \lesssim +350°$ and $-4.5° \lesssim b \lesssim -2.25°$, totalling ~266 sq. deg. To cover the area, $83 \times 2 = 166$ tiles were needed, with the tile names ranging from e0601 to e0766.
- High Extended Disk (Disk-high): symmetrical area to the Low Extended Disk at higher latitudes, $+230° \lesssim l \lesssim +350°$ and $+2.25° \lesssim b \lesssim +4.5°$, comprising ~ 266 sq. deg. Tile names range from e0767 to e0932.
- Disk to longitude +20 (Disk20): extended the disk coverage to the north within $+10° < l < +20°$ and $|b| \lesssim 4.50°$. A total of $7 \times 8 = 56$ tiles were used to fill the area of ~90 sq. deg. The area has ~ 90 sq. deg. Tile names in this region are e0933 to e0988.
- Disk to longitude +230 (Disk230): extended area to the southern disk coverage within $+230^{\rm o} < l < +295°$ and $|b| \lesssim 2.25°$. This is the largest new area, with ~292 sq. deg. A total of $45 \times 4 = 180$ tiles are in this region and labelled from d1001 to d1180.
- Low extended bulge (bulge-low): extended the bulge area within $-15° < b < -10°$ and $|l| \lesssim 10°$ with ~ 90 sq. deg. in size. There is a total of $14 \times 4 = 56$ tiles, labelled from b0401 to b0456.
- High Extended bulge (bulge-high): extended the bulge within $+5° < b < +10°$ and $|l| \lesssim 10^{\rm o}$. The area has also ~90 sq. deg. A total of $14 \times 4 = 56$ tiles filled the area and are named from b0457 to b0512.

The VVVX footprint along with the VVV original coverage is shown in Fig. 1, along with a comparison with other complementary surveys, while the list of the tile names with the central coordinates are presented in Appendix A (first ten rows) and in electronic form[4]. Both VVV and VVVX have a total of 1028 tiles. There are no tiles with names d0153–d0200, b0397–b0400, b0513–b0600 and d0989–d1000. The absence of tile numbers is attributed to the naming conventions, which are based on the regions covered by the tiles. The new VVVX areas added up to ~2000 h of observations, split between ~450 h for $JHK_{\rm s}$ and ~1550 h for the multi-epoch $K_{\rm s}$.

## 4. Observing strategy

The VVVX survey was carried out in service mode, which is the standard for all VISTA observations. The observational blocks (OBs) were prepared by the VVVX team using the P2PP/P2 tools[5] and sent to ESO for validation and observation at the site.

**Table 2.** Total exposure time for the VVVX observations.

| Filter | DIT (s) | NDIT | Njitter | Exposure time per pixel (s) |
|---|---|---|---|---|
| $J$ | 10 | 3 | 2 | 120 |
| $H$ | 6 | 2 | 2 | 48 |
| $K_{\rm s}$ | 4 | 1 | 2 | 16 |

**Notes.** For each OB the DIT is the detector integration time, NDIT is the number of the detector integration time, and Njitter is the number of offsets executed at each of the six pawprint positions. Njitter=2 applies for most of the tile area. Due to the tiling process, for a small fraction of ~8% of the tiles, the Njitter varies from Njitter=1 (at the edges) to Njitter=3, 4 or 6 (in the regions where the pawprints overlap). For details about the tile areas covered for each Njitter value, see Fig. 20 in VISTA/VIRCAM user manual (Ivanov et al. 2021).

Observing blocks for each tile were defined for: a single $K_{\rm s}$ band observation (used in the variability campaign), multicolour $JHK_{\rm s}$ observations (in a quasi-simultaneous schema: ~10 min for the sequence $H \rightarrow K_{\rm s} \rightarrow J$), and additional $J$ band observations to be combined for the multicolour observations. Due to scheduling constraints the multicolour observations had to be split into two separate observing blocks, including $JHK_{\rm s}$ and $J$ band observations, respectively. We note that depending on the region, between 2 and 8 adjacent tiles were combined in a concatenation and observed back-to-back. Minimum concatenation of 2 tiles was necessary to achieve a satisfactory background sky subtraction, and at the same time it reduced observational overheads.

All observations were carried out using a 2-point dither due to the variable and high sky background in the near-IR and to enable cosmic rays rejection and pixel defect correction. As a consequence, the total time per OB for an individual source (e.g., star) and filter is: DIT (detector integration time) × NDIT (number of detector integration time) × Njitter=2 (number of offsets executed at each of the six pawprint positions) × Npaw=6 (number of pawprints that together make a tile). These OB setups lead to a total time on the source in each OB of 120 s ($J$), 48 s ($H$) and 16 s ($K_{\rm s}$), as presented in Table 2.

The number of epochs observed during the VVVX campaign in each of the new areas ranged between 23 and 50 epochs (see Appendix A). In the original VVV region, typically 3–12 new epochs were acquired by the VVVX campaign, except in the inner Galactic bulge, where in a few tiles up to 100 additional epochs have been secured. In the region around the Baade's window, eight tiles covering ~13 sq. deg. in the VVV bulge reached up to 352 epochs, summing up the VVV and VVVX variability campaigns. Figure 2 shows the number of epochs observed for each tile while Fig. 3 illustrates the cadences for the $K_{\rm s}$ band variability campaign across the original VVV bulge area. Due to our flexible observing strategy, the observational sequence for all tiles is different, and the ranges of time separations between observations are also variable from tile to tile. Therefore, for variability studies, we recommend that each tile should be treated separately, as, for example, aliasing in the periods are tile dependent.

[3] https://www.eso.org/sci/observing/phase2/SMGuidelines/SADT.html

[4] The full table with the tile names and the central coordinates is available at https://zenodo.org/records/12587535

[5] https://www.eso.org/sci/observing/phase2/p2intro.html

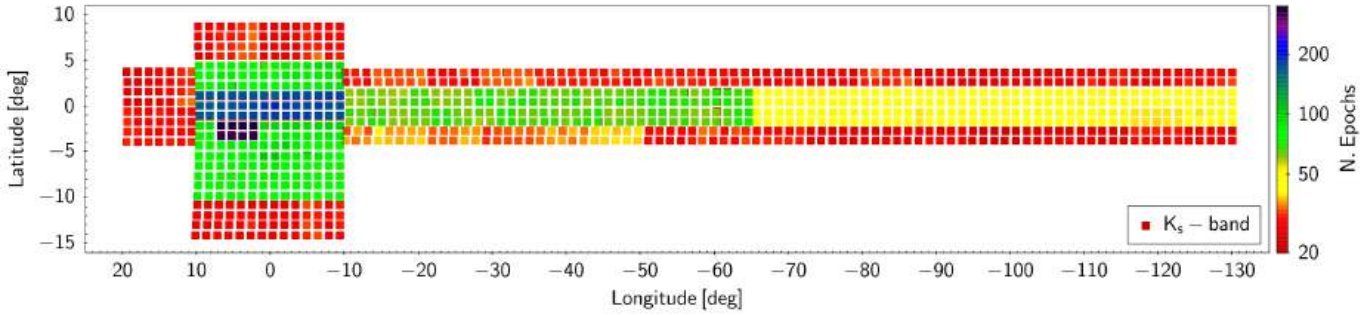


**Fig. 2.** Number of epochs in the $K_s$ band observed by VVV+VVVX. The mean baseline for the original area is ∼12 yr, with up 352 epochs for selected tiles in the inner bulge. For the outer bulge and disk the number of epochs are in the range 23–106 for the VVVX observations solely, varying according with the observational strategy.

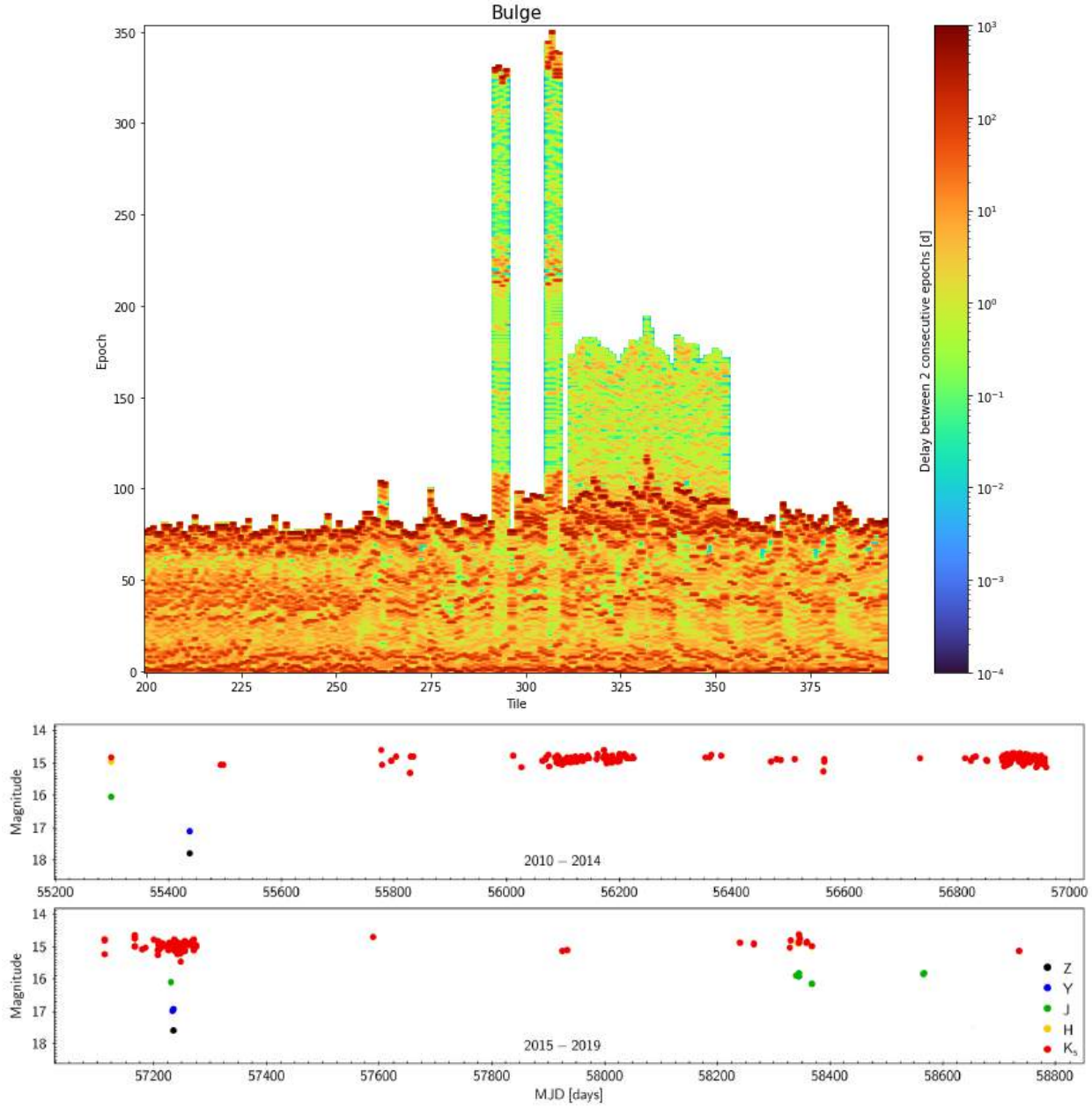


**Fig. 3.** Cadence of the VVV+VVVX bulge observations. Top: density plot showing the cadence of the bulge observations in both VVV and VVVX campaigns. Bottom: light curve example for the source VVV-VIVACE ID 533558 ($K_s$ ∼ 14.9 mag; Molnar et al. 2022), observed by VVV+VVVX in the five VISTA broad band filters in the bulge field b307. There are a total of 363 observations in the five filters along years 2010 to 2019. The coordinates for the target are RA, Dec (J2000) = 18:00:11.48, −28:25:13 (corresponding to $l, b$ = 2.0688, −2.4904 deg.).

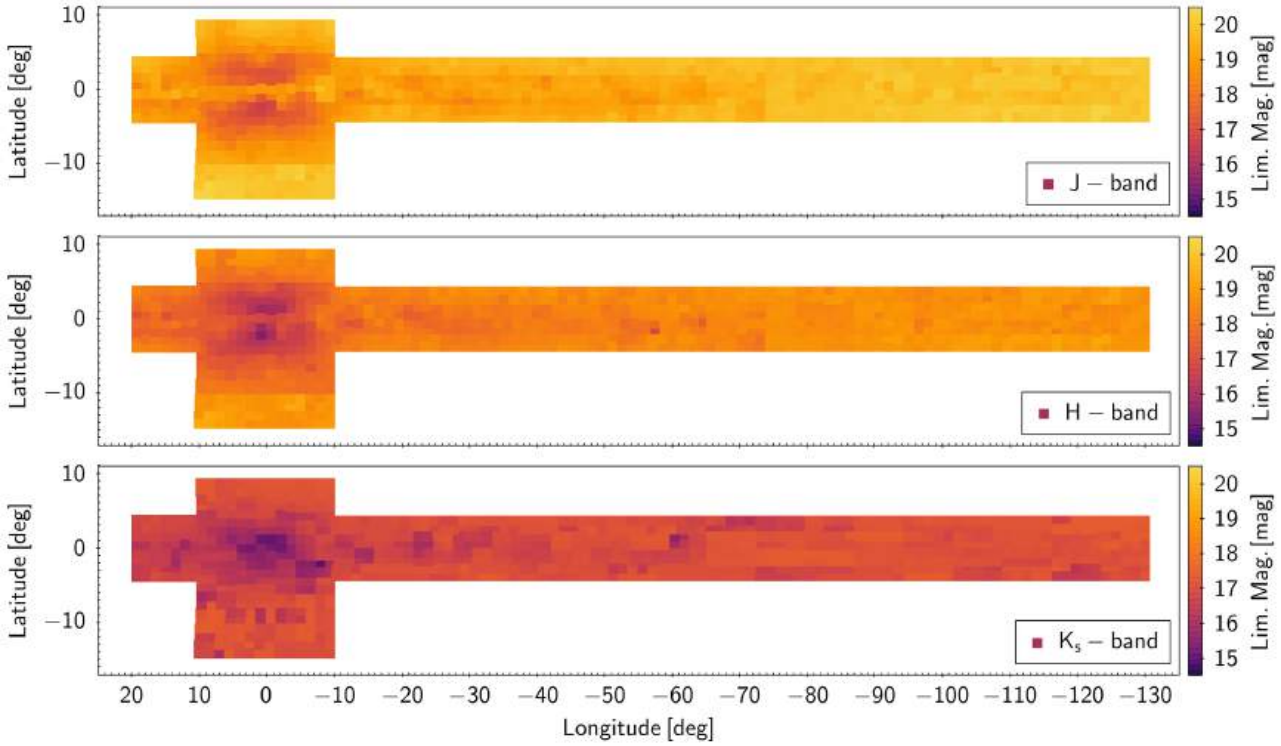


**Fig. 4.** 5$\sigma$ magnitude limits of the catalogues in the $J$, $H$, and $K_s$, respectively, from top to bottom. The colour scale is the same in the three panels as shown in the vertical bars at the right. For the $J$ and $H$ bands, VVV and VVVX are combined because of the lack of VVVX observation in these bands in the original VVV area.

$J$ filter only OBs were observed in order to double the exposure time in that filter. The deep $J$ imaging corresponds to a time on source of ∼4 min, and due to the 1 h restriction on OB duration, these additional $J$ filter observations had to be separate from the $JHK_s$ observations, for a given tile. The two $J$ images for each tile can be coadded to increase the useful depth of $K_s$ vs. $J - K_s$ colour magnitude diagrams. For instance, the combined $K_s$ epochs and the deep $J$ will reach $J = 20.8$ mag, $K_s = 20$ mag at 5$\sigma$, which is three magnitudes fainter than the unreddened bulge main-sequence turnoff. The densest fields will be confusion-limited, but applying both point-spread function (PSF) fitting techniques and differential photometry (DIA), it is possible to recover most objects down to $J = 19.5$ mag, $H = 18.5$ mag and $K_s = 18$ mag, even in fairly crowded fields. This is more than 3 mag fainter than the unreddened RR Lyrae in the Galactic bulge.

Contemporaneous $JHK_s$ epochs give the colours for variable stars (essential for precise dereddening of RR Lyrae and Cepheids) while the deep $J$ observations allow the construction of deep colour-magnitude diagrams reaching past the age-sensitive main sequence turn-off. Because denser fields are confusion-limited, the limiting magnitudes vary along the area, especially in the innermost bulge area. Figure 4 shows the limiting magnitudes as a function of position for all the filters.

The $J$ and $H$ observations were ≳85% and ≳95% complete by the end of the 2018 and 2019 season, respectively. The median image quality in $J$ and $H$ are 0.88″ and 0.84″ for a median airmass of 1.19 and 1.17, respectively, measured on combined tile images (see Fig. 5). The image quality is measured from the average FWHM of sources classified as bona fide stars with high signal-to-noise. This value includes atmospheric, telescope and instrument related aberrations and is not the same as seeing, which is an inherent property of the atmosphere independent of the telescope (Martinez et al. 2010). We refer to Sutherland et al. (2015) for a detailed description of the image quality design and performance of the VIRCAM@VISTA. In $K_s$, the observations exceeded ≳90% completeness only in 2022, with median image quality of 0.93″ for a median airmass of 1.21. In most cases the observations satisfied the atmospheric turbulence and photometric image quality parameters and were classified as completed. Remaining $JH$ observations were taken during 2020–2022 and $K_s$ in 2020–2023 to complete the planned observations within the photometric and image quality parameters.

We summarise in Table 3 the observed areas along the years of the VVVX campaign. Regarding the multicolour data, the $JHK_s$ observations were ≳94% complete by the end of the 2019 season. The remaining observations were secured during 2020–2023 and comprised repeated observations of the tiles that did not pass the quality control in the first instance. The cumulative distributions for the $JHK_s$ are presented in Fig. 6.

The VVVX observations were pipeline-processed at the Cambridge Astronomical Survey Unit (CASU), using the VISTA data flow system (VDFS) pipeline (Lewis et al. 2010). CASU also produces the photometric calibration of stacked pawprint images and tile images (González-Fernández et al. 2018). Multiband catalogues have also been generated by the VISTA Science Archive (VSA). All tiles, their confidence maps and extracted source lists, in addition to the corresponding pawprints, were processed with version 1.5 of the CASU pipeline. In the catalogues provided by CASU, a flag is used to indicate the most probable morphological classification. These flags were derived from the curve-of-growth analysis of the flux from different aperture sizes (Irwin et al. 2004). The flags are:

- '−1' to denote stellar objects,
- '−2' to denote borderline stellar,
- '−7' denoting sources containing bad pixels,

**Table 3.** Summary of the VVVX observational campaign.

| Area name | Area ($deg^2$) | No. of Tiles | RA Range (h) | 2016 | 2017 | 2018 | 2019 | 2020 | 2021 | 2022 | 2023 |
|---|---|---|---|---|---|---|---|---|---|---|---|
| VVV bulge | 313 | 196 | 17h−19h | $K_s$ | $K_s$ | $JHK_s$ | $JK_s$ | – | $K_s$ | $K_s$ | – |
| VVV disk | 232 | 152 | 12h−19h | $K_s$ | $K_s$ | $K_s$ | $K_s$ | – | – | $K_s$ | – |
| Disk Long. +20 | 90 | 56 | 18h−19h | $K_s$ | $JHK_s$ | $K_s$ | $K_s$ | – | – | $K_s$ | – |
| Disk Long. +230 | 292 | 180 | 07h−12h | – | – | $JHK_s$ | $K_s$ | $K_s$ | $K_s$ | $K_s$ | $K_s$ |
| Low Ext. Bulge | 90 | 56 | 18h−19h | $JHK_s$ | – | $K_s$ | $K_s$ | – | – | – | – |
| High Ext. Bulge | 90 | 56 | 17h−18h | $K_s$ | $JHK_s$ | $K_s$ | $K_s$ | – | – | $K_s$ | – |
| Low Ext. Disk | 266 | 166 | 07h−18h | $K_s$ | $JHK_s$ | $JHK_s$ | $JHK_s$ | $K_s$ | $K_s$ | $K_s$ | $K_s$ |
| High Ext. Disk | 266 | 166 | 07h−17h | $K_s$ | $JHK_s$ | $JHK_s$ | $JHK_s$ | $K_s$ | $K_s$ | $K_s$ | $K_s$ |

**Notes.** $J$ and $H$ observations were 97% and 94% completed by the end of 2019 season. The remaining observations were taken from 2020 to 2023, mostly repeated observations. The $K_s$ band was ≳99% completed by the end of the 2022 season. Only residual $K_s$ observations, comprising ≲1% of the total, were taken in year 2023 to complete the planned observations.

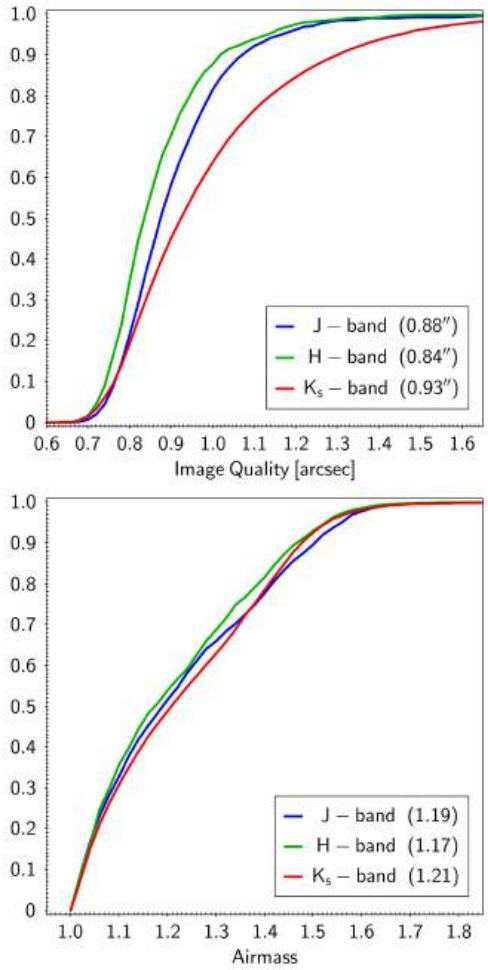


**Fig. 5.** Image quality and airmass cumulative distributions for the $JHK_s$ VVVX observations, in the top and bottom panels, respectively. The median values of image quality and airmass for each filter are presented in the legends.

- '−9' is used for saturated stars,
- '+1' is used for non-stellar objects and
- '0' is used to denote a noise measurement.

The entire reduction and calibration process is same as that applied to the VVV data. For more details on data processing and catalogue generation, we refer the reader to Sects. 2 and 3 of the VVV DR1 paper (Saito et al. 2012) and the references therein.

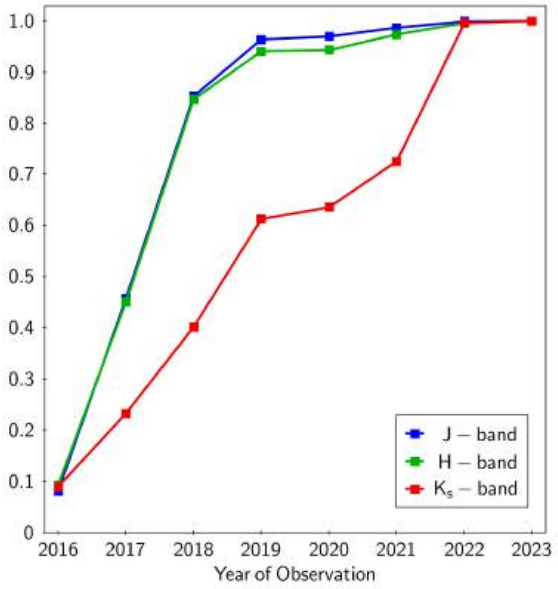


**Fig. 6.** Cumulative distributions for the $JHK_s$ observations during the VVVX campaign.

## 5. Previous data releases

The first VVVX data release (VVVX DR1[6]) was published in February 2019 and contains data acquired between July 2016 and August 2017. The first release contains observations of about 590 sq. deg., typically covered in the three filters ($J$, $H$ and $K_s$). DR1 released a total of 1660 tile images that passed quality control, plus their associated weight maps and single-band source catalogues. Moreover, it contains 9960 pawprint images and their associated weight maps that were used to create the tile images. The total data volume is about 1.7 TB in compressed format (CFITSIO RICE compression[7]).

[6] https://www.eso.org/rm/api/v1/public/releaseDescriptions/130
[7] http://wsa.roe.ac.uk//qa.html#compress

In June 2021, we publicly released the VVVX DR2[8] with the data taken between April 2018 and October 2019. They consist of both multicolour $JHK_s$ observations and $K_s$ band variability data. The DR2 has 10776 tile images, plus their associated single-band source catalogues and weight maps. For the pawprints, there is a total of 64 716 images, plus the single-band source catalogues and weight maps. The total data volume is eight times larger than DR1, reaching 13.4 TB in compressed format. The uncompressed data volume of the VVVX DR1 plus VVVX DR2 is $\gtrsim$27 TB.

The $K_s$ band taken prior to April 2018 was not released with the VVVX DR1, which contained data only from the multicolour $JHK_s$ OBs and $J$-only OBs. $JHK_s$ and $J$-only OBs taken during 2020–2022, as well as $K_s$ from 2020 to 2023, represent a smaller part of the total volume. These data had been gradually processed by CASU and VSA, and ingested to the ESO Archive, with no announcement of a public data release. These remaining data complete the release to the astronomical community of all the observations planned by VVVX within the established quality criteria. In total, the VVV+VVVX survey observations comprise >350 000 images, which including images, catalogs and confidence maps, they make a total of more than $10^6$ files.

The VVVX data, as described above, can be downloaded directly via the ESO Archive[9]. Various options are available for how the data can be obtained, from simple cone searches to more complex options. In the ESO Archive it is also possible to browse the VVVX data using an Aladin Sky Atlas tool, and by clicking and selecting, determine which data among images and catalogues are of interest for direct download.

## 6. Advanced data products

The images and catalogues described in the section above, already available via the VSA and ESO Archive, are being complemented by advanced products, currently under preparation by VVVX science team members. As for VVV, a key product is the extraction of PSF photometry, which is more robust and accurate than aperture photometry data for the regions of high crowding of stars, such as in the innermost MW bulge and plane, and for the study of star clusters (e.g. Alonso-García et al. 2018).

PSF-based catalogues are compiled for each VVVX tile, however measured from the stacked pawprint images, where codes such as DAOPHOT (Stetson 1987), DOPHOT (Schechter et al. 1993), and SExtractor (Bertin & Arnouts 1996) work with better precision.

As well as for the VVV Survey, various authors will provide independently produced PSF based source catalogues of the multicolour data (e.g. Alonso-García et al. 2018; Surot et al. 2019), and the variability campaign (e.g. Contreras Ramos et al. 2017; Smith et al. 2018). Specific details will be published elsewhere. The catalogues will be available through the VSA[10], using the same schema as for aperture and image data.

The $K_s$ band variability data allows for a variety of uses, from constructing light curves to proper motion measurements. For the VVV area, our team published a number of catalogues containing hundreds of thousands candidate of variable stars, for example: the VVV Near-IR Variability Catalogue (VIVA-I; Ferreira Lopes et al. 2020), the Near-IR Catalogue of known variable stars (Herpich et al. 2021), and the VIRAC Variable Classification Ensemble (VIVACE; Molnar et al. 2022).

The extinction in $K_s$ filter of VIRCAM is an order of magnitude lower than in optical. Hence, the VVVX proper motion data are complementary to those of *Gaia* in highly extincted Galactic disk and bulge regions, where the optical *Gaia* data result in significantly reduced depth. Over the area of the original VVV region, the $K_s$ band data can be combined to increase the time baseline to more than a decade ($\gtrsim$2010–2020, or even 2022 for selected bulge fields), thus increasing the accuracy of the proper motion measurements. For the new extended area, the time base is approximately 4–5 yr.

Proper-motion catalogues will be incorporated into the VISTA Infrared Catalogue 2 (VIRAC2, in preparation), the latest version of the original VISTA Infrared Catalogue (VIRAC; Smith et al. 2018). Luna et al. (2023) compared the VIRAC2, *Gaia* DR3 and HST proper motions in a few fields towards the Galactic bulge, with different stellar crowding levels. The test showed that VIRAC2 proper motions have more reliable uncertainties than *Gaia* DR3 and are comparable to HST in dense fields, such as globular clusters and the Galactic bulge. The shorter time base of the new VVVX areas should influence the data quality, so we should expect larger fractional uncertainties for more distant and slower sources. VIRAC2 has been uploaded to ESO archive where it will be available for Virtual Observatory (VO) TAP queries.

Aside from the aperture and PSF photometry for the point sources, the images also contain extended sources. The optical detection of extragalactic sources beyond the MW is hampered in the ZoA, where the stellar crowding and Galactic absorption are rather extreme (see Sect. 8.3).

## 7. Examples of data usage: Tile e1084, Carina Nebula, and NGC 3324

### 7.1. Multicolour images and catalogues

One of the first images released by the JWST is of the Carina Nebula[11]. The nebula is located within the Disk to Longitude +230 area, in tile e1084, which has central coordinates RA, Dec (J2000) = 10:30:32.86, −58:39:41.8, corresponding to $l, b = -74.524725, -0.649149$ deg. The $JHK_s$ observations of tile e1084 were carried out on March 19, 2018. Table 4 summarises the observational log. A composite false colour image combining the $JHK_s$ images can be produced with the Aladin Sky Atlas[12] for e1084 using the WCS data in the reader of each image to determine their location, rotation and image scale.

In Fig. 7, we compare the three colour $JHK_s$ image obtained with VISTA/VIRCAM with its JWST/NIRcam counterpart. Both images have $\sim 9 \times 7$ arcmin size, with a different orientation than equatorial or Galactic coordinates. JWST composite image comprises separate exposures containing F090W, F187N, F200W, F335M, F444W, F470N NIRCam narrow and wide filters. These filters are part of both the short and long wavelength channels, covering wavelengths from 0.901 to 4.707 microns, corresponding to pixel scales of 0.031″pixel$^{-1}$ and 0.063″pixel$^{-1}$ for the short and long wavelength channels, respectively. Although the JWST images were taken at a broader

[8] https://www.eso.org/rm/api/v1/public/releaseDescriptions/181
[9] http://archive.eso.org/cms.html
[10] http://vsa.roe.ac.uk/
[11] https://www.nasa.gov/image-feature/goddard/2022/nasa-s-webb-reveals-cosmic-cliffs-glittering-landscape-of-star-birth/
[12] https://aladin.cds.unistra.fr/

**Table 4.** Multicolour observations of tile e1084.

| Band | Obs. date (2018-03-20UT) | Airmass | Exp. time (s) | Seeing (″) | ZP (mag) | Maglim (mag) | N-sources | N-flags −1 | +1 | −2 | (sum) |
|---|---|---|---|---|---|---|---|---|---|---|---|
| $H$ | 06:35:58.7520 | 1.494 | 24.00 | 0.72 | 23.71 | 18.72 | 998,946 | 605,248 | 314,151 | 65,572 | (98.6%) |
| $K_s$ | 06:41:43.4729 | 1.514 | 8.00 | 0.73 | 22.88 | 17.17 | 592,401 | 338,805 | 229,305 | 18,006 | (98.9%) |
| $J$ | 06:45:19.4624 | 1.527 | 60.00 | 0.74 | 23.61 | 19.95 | 1,013,278 | 641,619 | 288,262 | 72,230 | (98.9%) |

**Notes.** Observational log and catalogue information for the multicolour observations of the VVVX tile e1084. All observations were labelled as 'Completed' and 'ESO Grade A'. The catalogues are dominated by stellar (−1), non-stellar (+1) and borderline stellar (−2) sources, accounting for ∼99% of the total number in each catalogue.


**Fig. 7.** VVVX composite image of the Carina Nebula compared with the JWST image of the same field. The VVVX image (top) is in false colour and based on the $JHK_s$ observations while the JWST image (bottom) comprises separate exposures containing F090W, F187N, F200W, F335M, F444W and F470N NIRCam filters. The Carina Nebula is located towards tile e1084 in the Disk to Longitude +230 region of VVVX, with the $JHK_s$ observations secured on March 19, 2018. The images have $\sim 9 \times 7$ arcmin size and are oriented with the north to the right and east to the top. Credits (JWST image): NASA, ESA, CSA, and STScI, J. DePasquale (STScI).

range of longer wavelengths (0.90–4.70 μm compared to 1.25–2.15 μm for VISTA), the VVVX images are comparable in quality for relatively bright point sources, while the nebular structure definition is clearly superior in the JWST. For faint sources, the higher resolution of JWST compared to VISTA allows the first to reach several magnitudes deeper at the same wavelengths.

Near the Carina Nebula (Fig. 7) we find NGC 3324, a stellar cluster first described by Kharchenko et al. (2005), based on PPMLX and 2MASS data. As described before VVVX offers NIR data not only with a much better resolution, but also reaches several magnitudes deeper. In Fig. 8 we present the $J$, $H$ and $K_s$ band images for the cluster. It is possible to note the difference in the gas transparency towards longer wavelengths, especially in the lower part of the images where the gas concentration is higher, increasing the number of background sources that can be observed.

We created a multicolour catalogue for tile e1084 by cross-matching the $J$, $H$ and $K_s$ band catalogues provided by CASU (aperture photometry, see Table 4). For the cross-match

**Fig. 8.** Individual $J$ (left), $H$ (centre) and $K_s$ band images (right) of the star cluster NGC 3324. The image is centrered at RA/DEC (J2000)=10:37:21.8, −58:36:54, with 9 arcmin side and oriented in Galactic coordinates.

procedure we made use of STILTS[13] (Taylor 2006), allowing a tolerance of 1″ between the sky coordinates of the detected sources, resulting in a $JHK_s$ band catalogue with 568k sources, which is limited by the shorter exposure time in the $K_s$ band compared with the other filters (see Table 2). Multiepoch $K_s$ band images can be coadded to provide a deeper catalogue; however, that has not been applied here. In using the photometric flags and selecting only stellar sources in all 3 bands (flag '–1', see previous section), the number of sources in the e1084 catalogue dropped from 568k to 262k sources. The $J \times (J - K_s)$ CMD of stellar sources in tile e1084 is presented in Fig. 9. We have also similarly prepared CMDs for the region of Carina and NGC 3324, for the same areas presented in Figs. 7 and 8.

In order to demonstrate the importance of the PSF photometry, we also present CMDs using PSF data for the same regions mentioned above: tile e1084, the Carina Nebula region, and NGC 3324. We are currently finishing the PSF atlas for the whole VVVX area (Alonso-García et al. in prep.), building on our previous experience extracting the PSF photometry from the original VVV footprint (Alonso-García et al. 2018). A preliminary version of the PSF catalogues was used to build the CMDs of these areas of interest in Fig. 9.

Although there is excellent agreement between the aperture and PSF photometries, a larger number of sources in the PSF catalogues is evident since our algorithm to extract the PSF photometry uses a less conservative limit than the CASU aperture photometry. This difference becomes larger for the more crowded fields over the Galactic plane where the PSF is far more efficient. The VVVX PSF catalogues for the entire area will be described in Alonso-Garcia et al. (in prep.) and publicly released to the community through VSA.

### 7.2. Variability data: Light curves and proper motions

Dékány et al. (2013) present the effects of the time-domain sampling on the detection efficiency of variable stars. They showed that even a random cadence in the observations will allow us to detect RR Lyrae and $\delta$-Cepheids at $K_s$=14 mag unambiguously, provided a minimum number of 25 epochs. Therefore, between 25–40 individual $K_s$ band observations were allocated to the new extended survey area. More frequent observations (40 epochs) were assigned to more highly reddened regions in the new VVVX disk area at $230° < l < 295°$ (see Fig. 2), given that fainter variable stars require a larger number of observing epochs, and distant parts of the Galactic disk lie mainly in reddened, low latitude regions. Moreover, the number of epochs also depends on the type of variable star we expect to find in each region; for short-period variables, a greater number of epochs is required. Similarly, we have simulated the gain in proper motion precision of VVVX, relative to VVV. We find that 10 epochs offers the best compromise between precision and time spent, yielding an uncertainty of 300 $\mu as\,yr^{-1}$ thanks to the 9.5 yr baseline. This very high precision is essential to enable high quality decontamination of star clusters to $K_s$ = 15–16 mag in very crowded inner Galaxy fields and our goal of 5D mapping of Galactic structure. VVVX astrometry in VIRAC2 is placed on the *Gaia* absolute astrometric reference frame, which is very precise even in the plane due to the *Gaia* method of simultaneously observing two widely separated fields.

With the long time-baseline, the high precision proper motion measurements can disentangle the bulk bulge/disk stellar motions, producing a global pure bulge/disk colour-magnitude diagram (Libralato et al. 2015). As the innermost regions of the MW bulge and central disk remain out of reach for *Gaia* observations due to their high dust extinction, it will be up to VVV and VVVX to provide input catalogues for spectroscopic surveys such as MOONS, the Milky Way Mapper (MWM; Kollmeier et al. 2017) and others.

The observing strategy for e1084 consists in 41 $K_s$ band epochs over a baseline of 4-years, which allows the search and study of various classes of variable and transient stars, including pulsating variable stars used as distance indicators, such as RR Lyrae and Cepheids. The complete set of $K_s$ band source catalogues for tile e1084 were matched following the same procedure as for the multicolour catalogue in order to construct the light curves for the tile. Figure 10 shows the light curves derived and subsequently phase folded for two previously known RR Lyrae stars discovered by *Gaia* in the region of tile e1084 (Rimoldini et al. 2023).

By applying a Lomb–Scargle (LS) algorithm (Lomb 1976; Scargle 1982; Zechmeister & Kürster 2009) we detected the periodic signal, albeit in the case of *Gaia* DR3 5255393833932660992 with the double period, which is a common feature in this type of analysis (e.g. Catelan et al. 2013; Ferreira Lopes et al. 2020; Botan et al. 2021). This factor-of-two error in the period determination is a well-known issue that affects the LS method (and its variants) when faced with nearly sinusoidal light curves, both in the near-IR as in the optical (e.g. Graham et al. 2013, 2017; VanderPlas 2018). In applying the string length minimisation method

[13] https://www.star.bris.ac.uk/~mbt/stilts/

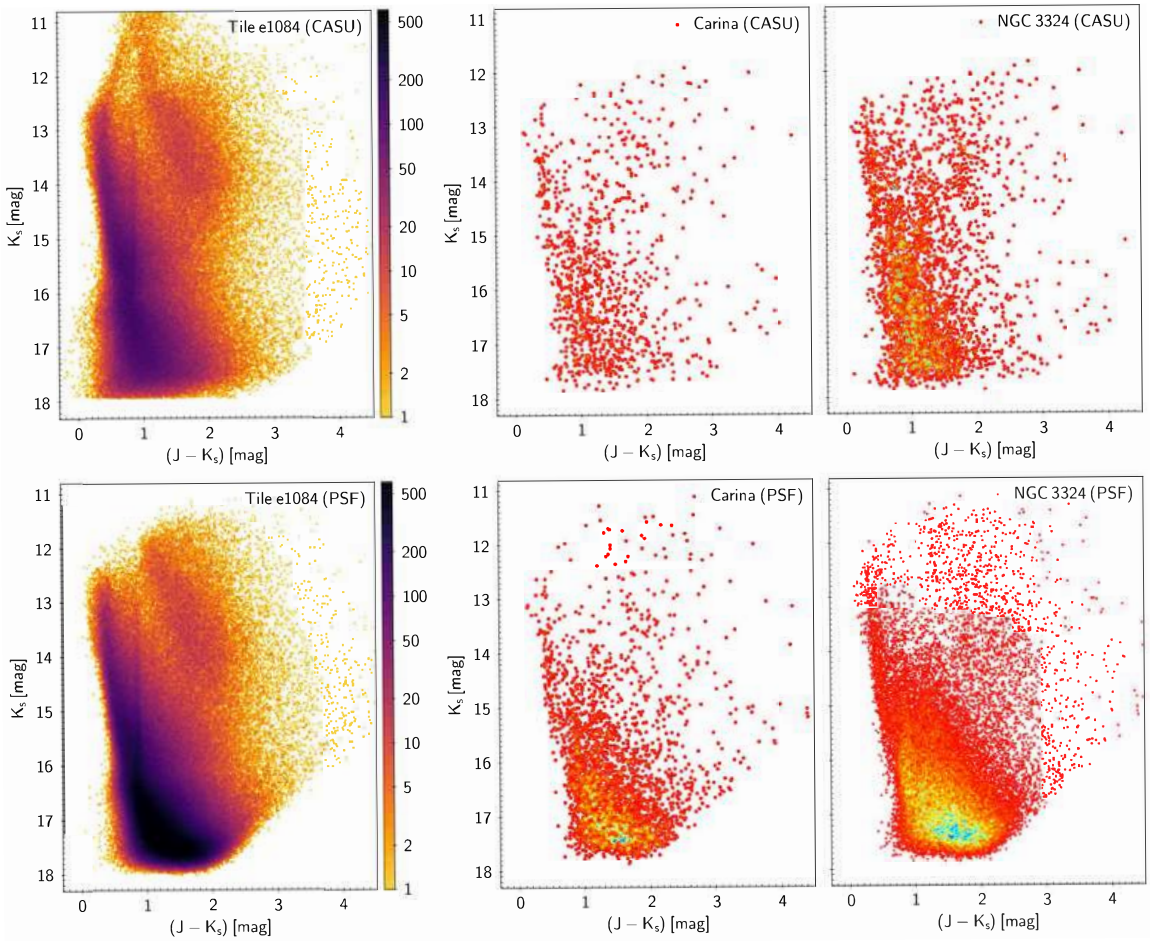


**Fig. 9.** Comparative $K_s \times (J - K_s)$ colour-magnitude diagrams. Top: CASU aperture photometry for stellar sources (flag −1) for the entire e1084 tile (left), for the region of the Carina Nebula shown in Fig. 7 (centre) and for the stellar cluster NGC 3324 (right panel, 6 arcmin radius area). The sharp end at $K_s = 17.9$ is caused by the stellar flag criterion applied. Bottom: the CMD for the same areas in the top using PSF photometry. In the CMDs for the entire tile, the narrow and vertical structure seen at $(J - K_s) \sim 0.9$ is the sequence of unreddened nearby M dwarfs (e.g. Alonso-García et al. 2018; Mejías et al. 2022).

(Burke et al. 1970; Dworetsky 1983; Clarke 2002), periods of 0.4763 days and 0.2380 days were obtained for *Gaia* DR3 5255393833932660992 and *Gaia* DR3 5255378372049581568, respectively, in agreement with those reported in the literature.

We emphasise that aperture data is not ideal for studying variability in crowded fields, and PSF data is more desirable, or even differential imaging analysis (DIA), in order to obtain more accurate photometry and thus reduce the scattering on the light curves. We also note that there is a potential problem due to the different epochs having slightly different zero points, so it is necessary to recalibrate the different epochs to a reference zero point. This preliminary result using CASU aperture data shows that VVVX data will find variables even with a smaller number of epochs and a shorter time baseline compared to VVV, especially in the innermost disk ($|b| < 1$ deg), where surveys carried out in the optical, for instance by *Gaia* or the upcoming *Vera C. Rubin* Observatory with its 3200 megapixel camera, are highly affected by extinction.

As described above, the VIRAC catalogue with the proper motion measurements based on the PSF data should be available soon for the VVVX area. While VIRAC2 covers the original VVV area using VVV+VVVX observations from 2010–2019, VIRAC3 will cover the whole VVV+VVVX area. VIRAC3 is currently being generated.

Regardless, we applied a different method to the CASU aperture data, by subtracting the differences of the RA/DEC between the latest and the first epochs observed in $K_s$ for e1084 for $K_s < 16$ mag stellar sources ('−1' flag) in both epochs, without any other type of calibration or selection criteria. Even with this naive PM approach, the bulk motion is in agreement with that expected motion for stars in the Galactic disk (e.g. Gaia Collaboration 2023), with $\langle PM_{RA} \cos Dec \rangle = -6.40 \pm 5.46$ mas yr$^{-1}$ and $\langle PM_{Dec} \rangle = -1.53 \pm 5.02$ mas yr$^{-1}$ (see Fig. 11). Given that *Gaia* is severely limited in the inner disk areas, only about 40% of stellar sources as faint as $K_s > 16.0$ mag are detected, compared to the CASU source catalogues. These objects are likely the closest to us, that is, those with bluer colour in the CMD. Since *Gaia* does not reach the stars closer to the Galactic centre, VVVX and VVV are invaluable for PM studies in those areas. This is even more evident when comparing *Gaia* with PSF based source catalogues.

## 8. The VVVX science returns

A large public survey such as the VVVX is expected to have a broad impact in different areas of astrophysics. As useful references for the reader interested in using the VVVX database, in this section we briefly summarise the published works on

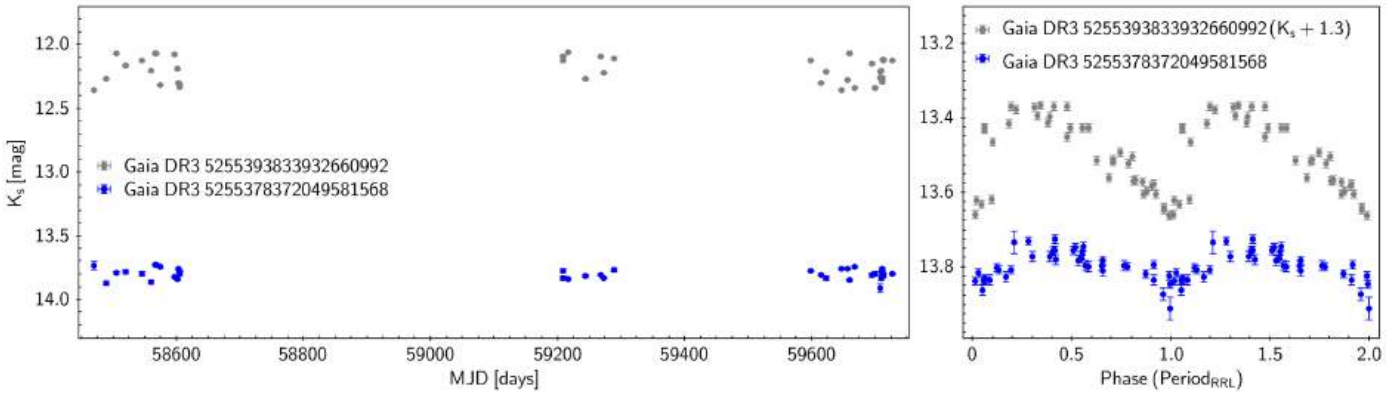


**Fig. 10.** VVVX $K_s$ band light curves for two *Gaia* RR Lyrae found in tile e1084. *Gaia* DR3 5255393833932660992 is a fundamental mode RR Lyrae (RRab) with a period of $P \sim 0.476$ days while *Gaia* DR3 5255378372049581568 is a first-overtone RR Lyrae (RRc) with $P \sim 0.238$ days. In the right panel, the phase folded light curve of *Gaia* DR3 5255393833932660992 is arbitrarily shifted by +1.3 mag for visualisation purposes.

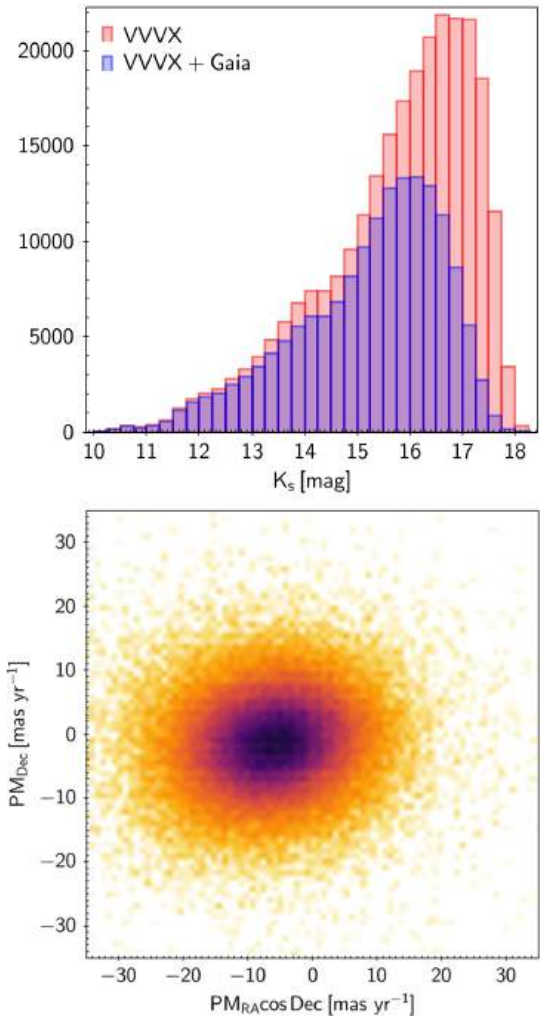


**Fig. 11.** Proper motion measurements for tile e1084. Top: histogram in $K_s$ band for stellar sources in both the first and latest $K_s$ band epochs observed for e1084. About 60% of the sources have counterparts in *Gaia* DR3. This number dropped to $\lesssim$40% for $K_s > 16.0$ mag. Bottom: Naive PM measurements based on the differences of the RA/Dec between the latest and the first epochs. The grid pattern is an artefact of the binning algorithm used for plotting, and is not a real feature. Only stellar sources with $K_s < 16.0$ have been used and the timespan is ~4.2 yr (1530 days). The mean values are $PM_{RA}\cos Dec = -6.40 \pm 5.46$ mas yr$^{-1}$ and $PM_{Dec} = -1.53 \pm 5.02$ mas yr$^{-1}$.

planetary, stellar, Galactic, and extragalactic astronomy, starting with those that include large-scale photometry and astrometry.

### 8.1. Photometry and astrometry

As discussed above, Alonso-García et al. (in prep.) will extend the near-IR atlas from the VVV footprint (Alonso-García et al. 2018) to the VVVX new surveyed regions in the Galactic plane, using PSF-fitting techniques to extract the photometry. Smith et al. (in prep.) will also extend the astrometric and multi-epoch photometric dataset from the original VIRAC catalogue (Smith et al. 2018) using PSF photometry and adding the new epochs provided by the VVVX.

### 8.2. Variable stars and Galactic astronomy

Regarding variable stars, Alonso-García (2021) described the potential of classical pulsators such as RR Lyrae, Type 2 Cepheids, and Classical Cepheids for tracing the structure of the inner Galactic bulge and Disk in the VVVX region. In addition, Daza-Perilla et al. (2023a) performed the automated classification of eclipsing binary systems discovered in the extended database, that are also useful tracers across the Galactic plane.

Molnar et al. (2022) performed a massive classification of variable stars across the Galactic bulge and disk using the VVV and VVVX survey data, automatically classifying 1.4 million point sources. In a follow-up study, Sanders et al. (2022) studied the Mira variable stars in the innermost regions of the MW, using these luminous variables as tracers of the nuclear stellar disk. This sample was also used to estimate the epoch of the Milky Way's bar formation using detailed dynamical modelling (Sanders et al. 2024).

More recently, Lucas et al. (2024) carried out a massive search for the highest amplitude infrared variables, discovering a number of eruptive protostars, a new class of variables named dipping giants, as well as a variety of other interesting sources (transients, LPVs, microlensing events, etc.), thus enabling a variety of follow up studies. For example, Guo et al. (2024) presented a detailed, unique multi-wavelength study of an ongoing FUor-type outburst. VVVX will enable to develop a unified picture of eruptive Young Stellar Objects (YSOs) by longer term monitoring of slow variables and long-lasting YSO eruptions, to bridge the eruption timescale gap between EXors (weeks-months) and FUors (>10 yr).

Large surveys also open the door for serendipitous discoveries, which often lead to new science (e.g. Wolf et al. 2024). In this context, Saito et al. (2023) reported the discovery of VVV-WIT-12, which appears to be a 4-yr-long period YSO that induces variability in its surrounding nebula, and discuss the different possible scenarios that include a light echo or a precessing circumstellar disk.

### 8.3. Background galaxies

The VVVX images are deep enough to see through the MW, also enabling studies of background galaxies in the ZoA. As an example, the Circinus galaxy is the nearest known Seyfert II galaxy, located at a distance $D = 4$ Mpc. Obasi et al. (2024) carried out a search for globular clusters (GCs) in the halo of the Circinus galaxy, discovering dozens of bonafide GC candidates.

More distant galaxies can also be traced. Baravalle et al. (2021) and Duplancic et al. (2024) discovered thousands of galaxies in the ZoA behind the MW disk and bulge, respectively, that are useful to complete the picture of large-scale structure in the region. Daza-Perilla et al. (2023b) published an extensive near-IR galaxy catalogue in the northern part of the Galactic disk using machine learning techniques for the first time in these regions. Also, Marchant Cortés et al. (2024) explored the classification (and misclassification) of galaxies performed by Zhang, Zhao, & Wu (2021) using machine learning tools in the 4XMM-DR9 database.

Clusters of galaxies were also discovered in the near-IR database. Galdeano et al. (2022) published a deep near-IR view of the Ophiuchus galaxy cluster, the second-brightest X-ray cluster of galaxies in the sky, after the Coma cluster. In addition, Galdeano et al. (2023) unveiled a new such structure behind the MW.

### 8.4. Low-mass stars and exoplanets

The VVVX near-IR database is also useful for studies in the area of low luminosity stars and sub-stellar objects (M dwarfs, white dwarfs, brown dwarfs, and giant planets). Mejías et al. (2022) presented deep VVVX near-IR photometry for 99 low-mass stars in the *Gaia* EDR3 Catalogue of Nearby Stars, very useful for the characterisation of individual objects and for the identification of new faint objects in our vicinity. Cáceres et al. (2024) reported the discovery of a dozen planetary-mass binaries in the Lower Centaurus-Crux association. Also, Ferreira et al. (2024) presented the study of a benchmark White Dwarf – Ultracool Dwarf wide field binary in the Galactic plane.

### 8.5. Star clusters

The VVVX depth and resolution permits to see deep into our own Galaxy (Minniti et al. 2024). Therefore, the database also enabled the discovery of numerous star clusters in the reddened and crowded regions of the Galactic disk and bulge.

The works of Borissova et al. (2018, 2019, 2020); Peña Ramírez et al. (2021, 2022) identified dozens of open star clusters, either new or known, using VVV(X) data, enriching their near-infrared cluster sequences. This allowed the authors to characterise the clusters at different mass ranges, probing the small scale star formation in the Galactic disk.

Numerous old globular cluster were also identified and characterised in the VVVX areas of the disk and bulge (Bica et al. 2018; Obasi et al. 2021; Gran et al. 2019, 2022; Garro et al. 2020, 2021a, 2022, 2023; Fernández-Trincado et al. 2021, Saroon et al. 2024) and in the Sagittarius dwarf galaxy located behind the bulge (Garro et al. 2021b; Minniti et al. 2021a). The near-IR photometry allows the determination of some important cluster parameters, such as reddening, distance, luminosity, metallicity, mass, structure, and age, contributing to the understanding of the Milky Way GC system as a whole (Minniti et al. 2021b, Garro et al. 2024).

### 8.6. Long timescale microlensing events

VVV has demonstrated its ability to detect microlensing events, particularly in highly obscured and crowded fields, where such events are more frequent (Navarro et al. 2017, 2018, 2020a,b). Long-duration microlensing events exceeding one year are excellent candidates for stellar mass black holes. The extended time baseline of VVVX observations will enable the discovery of such events around the Galactic centre and plane, where models predict the presence of stellar mass black holes (e.g. Bahcall & Wolf 1976; Freitag et al. 2006; Alexander & Hopman 2009).

## 9. Survey legacy

The VVV and VVVX surveys are the result of more than 4000 h of observation with the most advanced ground-based near-IR facility. Although VVV+VVVX had observed ~4% of the celestial sphere, the region contains the majority of the Milky Way's stars, as well as the largest concentration of gas and dust in the Galaxy.

There are currently no other near-IR projects with similar characteristics to VVV+VVVX, such as time-baseline, wavelength range, photometric depth, and most importantly, the large projected area. However, the legacy of both surveys is much enhanced by complementary data from DECaPS and Pan-STARRS (Chambers et al. 2016), that also cover the MW bulge and southern plane. Here we must also mention the complementary survey VISIONS (Meingast et al. 2023) that targets individual star forming regions in the MW.

In the future projects, such as the *Vera C. Rubin* Observatory which will use optical wavelengths for massive variability, it will also be very complementary. Also complementary are the JWST observations, with instruments covering a small field of view but with much higher resolution and depth (e.g., Sect. 7). However, it would be unfeasible for the JWST to cover large areas with the same efficiency as our survey.

Clearly, the VVVX survey also serves as a vast source of targets for spectroscopic follow-up with future infrared spectroscopic surveys such as MOONS, 4MOST, MWM and the ESO Wide-field Spectroscopic Telescope (WST; Mainieri et al. 2024). Our survey is also a source of targets for the various next-generation extremely large telescopes; and may only be surpassed in performance in the next decade by projects such as the *Nancy Grace Roman* Space Telescope, which will be able to produce deep infrared images of large regions, including the Galactic centre, with higher resolution from space (e.g. Paladini et al. 2023).

The VVVX (and VVV) legacy will last for many years to come. Despite the numerous results already obtained, the full exploitation of the data will take many years more, becoming more attractive with each new product that can be obtained, as detailed extinction (or even metallicity) maps, catalogues of variable sources and transient objects, and even studies of background galaxies, especially in the ZoA beyond the MW plane.

## 10. Summary

In March 2023, we finished successfully the VVVX survey observations that started in 2016, which represents a huge amount of data and processing, comprising ~200 000 images that monitor $>10^9$ sources in our Galaxy and beyond. This is quite an accomplishment for VISTA, for ESO's Paranal Observatory, for the CASU data reduction pipeline, for the teams extracting PSF photometry from the images, for the VISTA Science archive in Edinburgh and for the ESO archive: the successful VVVX observations are now 100% completed. We have described the survey, including the observations, areal and temporal coverage, reductions, photometry, and astrometry. We have also presented some specific scientific examples for database usage, providing some key useful references.

Clearly, there are many more applications of this ESO Public Survey for the community to exploit for future studies of Galactic structure, stellar populations, variable stars, star clusters of all ages, among other exciting research areas, from stellar and (exo)planetary astrophysics to extragalactic studies. The image processing, data analysis and scientific exploitation will continue for the next few years, with many discoveries yet to come. The VVVX Survey will also be combined with future facilities to boost its scientific outcome in unpredictable ways: we are sure that this survey will remain a goldmine for MW studies for a long time.

*Acknowledgements.* We gratefully acknowledge the use of data from the ESO Public Survey program IDs 179.B-2002 and 198.B2004 taken with the VISTA telescope and data products from the Cambridge Astronomical Survey Unit (CASU) and the VISTA Science Archive (VSA) and the ESO Science Archive. VVV and VVVX data are published in the ESO Science Archive in the data collections identified by the following DOIs: https://doi.eso.org/10.18727/archive/67 and https://doi.eso.org/10.18727/archive/68. R.K.S. acknowledges support from CNPq/Brazil through projects 308298/2022-5, 350104/2022-0 and 421034/2023-8. D.M. gratefully acknowledges support from the Center for Astrophysics and Associated Technologies CATA by the ANID BASAL projects ACE210002 and FB210003, by Fondecyt Project No. 1220724, and by CNPq/Brazil through project 350104/2022-0. J.A.-G. acknowledges support from Fondecyt Regular 1201490 and by ANID – Millennium Science Initiative Program – ICN12_009 awarded to the Millennium Institute of Astrophysics MAS. Support for J.B. and R.K. are provided by ANID's FONDECYT Regular grant #1240249; ANID's Millennium Science Initiative through grants ICN12_009 and AIM23-0001, awarded to the Millennium Institute of Astrophysics (MAS). C.C. acknowledges support by ANID BASAL project FB210003. N.J.G.C. acknowledges support from the UK Science and Technology Facilities Council. E.B.A. thanks Universidade Estadual de Feira de Santana for the support received by the Program FINAPESQ (project number 050/2021). L.R.B. acknowledges financial support by INAF under WFAP project, f.o.:1.05.23.05.05. J.I.A. acknowledges the financial support of DIDULS/ULS, through the project PR2324063. A.B. acknowledges support from the Deutsche Forschungsgemeinschaft (DFG, German Research Foundation) under Germany's Excellence Strategy – EXC 2094 – 390783311. B.D. acknowledges support by ANID-FONDECYT iniciación grant No. 11221366 and from the ANID Basal project FB210003. A.C.G. acknowledges support from PRIN-MUR 2022 20228JPA3A "The path to star and planet formation in the JWST era (PATH)" funded by NextGeneration EU and by INAF-GoG 2022 "NIR-dark Accretion Outbursts in Massive Young stellar objects (NAOMY)" and Large Grant INAF 2022 "YSOs Outflows, Disks and Accretion: towards a global framework for the evolution of planet forming systems (YODA)". J.A.C-B. acknowledges support from FONDECYT Regular N 1220083. Support for M.C. is provided by ANID's FONDECYT Regular grant #1171273; ANID's Millennium Science Initiative through grants ICN12_009 and AIM23-0001, awarded to the Millennium Institute of Astrophysics (MAS); and ANID's Basal project FB210003. M.C.C. acknowledges financial support from the Universidad Complutense de Madrid (UCM) and the Agencia Estatal de Investigación (AEI/10.13039/501100011033) of the Ministerio de Ciencia e Innovación and the ERDF "A way of making Europe" through projects PID2019-109522GB-C5[4] and PID2022-137241NBC4[4]. P.C. and E.S. acknowledge financial support from the Spanish Virtual Observatory project funded by the Spanish Ministry of Science and Innovation/State Agency of Research MCIN/AEI/10.13039/501100011033 through grant PID2020-112949GB-I00. V. Motta acknowledges support from ANID FONDECYT Regular grant number 1231418. J.G.F.-T. gratefully acknowledges the grants support provided by ANID Fondecyt Iniciación No. 11220340, ANID Fondecyt Postdoc No. 3230001 (Sponsoring researcher), from the Joint Committee ESO-Government of Chile under the agreement 2021 ORP 023/2021 and 2023 ORP 062/2023. Support for C.E.F.L. is provided by the ANID/FONDECYT Regular grant 1231637. D.G. gratefully acknowledges the support provided by Fondecyt regular no. 1220264. D.G. also acknowledges financial support from the Dirección de Investigación y Desarrollo de la Universidad de La Serena through the Programa de Incentivo a la Investigación de Académicos (PIA-DIDULS). The work of F.N. is supported by NOIRLab, which is managed by the Association of Universities for Research in Astronomy (AURA) under a cooperative agreement with the National Science Foundation. W.G. gratefully acknowledges funding from the European Research Council (ERC) under the European Union's Horizon 2020 research and innovation programme under grant agreement 951549 (project UniverScale). F.G. gratefully acknowledges support from the French National Research Agency (ANR) – funded projects "MWDisc" (ANR-20-CE31-0004) and "Pristine" (ANR-18-CE31-0017). Z.G. is supported by the ANID FONDECYT Postdoctoral program No. 3220029. E.L.M. is supported by the European Research Council Advanced grant SUBSTELLAR, project number 101054354. V.M. acknowledges support from project DIDULS Regular N$^o$ PR2353857. M.C. thanks the support of ANID BECAS/DOCTORADO NACIONAL 21110001. I.P. acknowledges support from ANID BECAS/DOCTORADO NACIONAL 21230761. G.P. acknowledges support from ANID through Millennium Science Initiative Programs ICN12 009. S.R.A. acknowledges support from Fondecyt Regular 1201490. E.S. acknowledges financial support from the Spanish Virtual Observatory project funded by the Spanish Ministry of Science and Innovation/State Agency of Research MCIN/AEI/10.13039/501100011033 through grant PID2020-112949GB-I00. D.S. acknowledged support from the Science and Technology Facilities Council (STFC, grant numbers ST/T007184/1, ST/T003103/1, ST/T000406/1 and ST/X001121/1). M.T. is supported by the JSPS Kakenhi No. 24H00242. P.B.T. gratefully acknowledge support by the ANID BASAL project FB210003 and Fondecyt 1240465. S.V. gratefully acknowledges the support provided by Fondcyt regular n. 1220264. SV gratefully acknowledges support by the ANID BASAL projects ACE210002 and FB210003. C.N.M. gratefully acknowledges support from the Research Department of the Austral University of Chile, Puerto Montt Campus (Project DIPM-CIB2303). Financial support for this work was also provided by the ANID BASAL Center for Astrophysics and Associated Technologies (CATA) through grants AFB170002, ACE210002 and FB210003, by the ANID Millennium Institute of Astrophysics (MAS) ICN12_009 and by ANID Fondecyt Regular 1230731 (PI: M.Z.). We are also deeply thankful to our dear colleague Rodolfo Barbá, who was a pillar for the survey but sadly passed away in late 2021, may he rest in peace.

## References

Alexander, T., & Hopman, C., 2009, ApJ, 697, 1861
Alonso-García, J. 2021, ASPC, 529, 199
Alonso-García, J., Saito, R. K., Hempel, M., et al. 2018, A&A, 619, A4
Arnaboldi, M., Delmotte, N., Gadotti, D., et al. 2019, The Messenger, 178, 10
Bahcall, J. N., & Wolf, R. A. 1976, ApJ, 209, 214
Baravalle, L. D., Alonso, M. V., Minniti, D., et al. 2021, MNRAS, 502, 601
Barbuy, B., Chiappini, C., & Gerhard, O. 2018, ARA&A, 56, 223
Bertin, E., & Arnouts, S. 1996, A&AS, 117, 393
Bica, E., Minniti, D., Bonatto, C., & Hempel, M. 2018, PASA, 35, e025
Blanton, M. R., Bershady, M. A., Abolfathi, B., et al. 2017, AJ, 154, 28
Borissova, J., Chené, A.-N., Ramírez Alegría, S., et al. 2014, A&A, 569, A24
Borissova, J., Ivanov, V. D., Lucas, P. W., et al. 2018, MNRAS, 481, 3902
Borissova, J., Ivanov, V. D., Lucas, P., et al. 2019, BAAA, 61, 110
Borissova, J., Kurtev, R., Amarinho, N., et al. 2020, MNRAS, 499, 3522
Botan, E., Saito, R. K., Minniti, D., et al. 2021, MNRAS, 504, 654
Burke, E. W., Rolland, W. W., & Boy, W. R. 1970, JRASC, 64, 353
Cáceres, C., Minniti, D., Mejías, A., et al. 2024, A&A, submitted
Cardelli, J. A., Clayton G. C., & Mathis, J. S. 1989, ApJ, 345, 245
Catelan, M., Minniti, D., Lucas, P. W., et al. 2011, RR Lyrae Stars, Metal-Poor Stars, and the Galaxy, 145
Catelan, M., Dekany, I., Hempel, M., & Minniti, D. 2013, BAAA, 56, 153
Chambers, K. C., Magnier, E. A., Metcalfe, N., et al. 2016, arXiv e-prints [arXiv:1612.05560]
Clarke, D. 2002, A&A, 386, 763
Contreras Ramos, R., Zoccali, M., Rojas, F., et al. 2017, A&A, 608, A140
Dalton, G. B., Caldwell, M., Ward, A. K., et al., 2006, SPIE, 6269, 62690X
Daza-Perilla, I. V., Gramajo, L. V., & Lares, M. 2023a, MNRAS, 520, 828
Daza-Perilla, I. V., Sgró, M. A., Baravalle, L. D., et al. 2023b, MNRAS, 524, 678
de Jong, R. S., Agertz, O., Berbel, A. A., et al. 2019, The Messenger, 175, 3
Dékány, I., Minniti, D., Catelan, M. 2013, ApJ, 776, L19
Drew, J. E., Gonzalez-Solares, E., Greimel, R., et al. 2014, MNRAS, 440, 2036

Duplancic, F., Alonso, S., Coldwell, G., et al. 2024, A&A, 682, A153
Dworetsky, M. M. 1983, MNRAS, 203, 917
Emerson, J. P., & Sutherland, W. J. 2010, Proc. SPIE, 7733
Emerson, J., McPherson, A., & Sutherland, W. 2006, The Messenger, 126, 41
Fernández-Trincado, J. G., Minniti, D., Souza, S. O., et al. 2021, ApJ, 908, L42
Ferreira, T., Saito, R. K., Minniti, D., et al. 2024, MNRAS, 527, 10737
Ferreira Lopes, C. E., Cross, N. J. G., Catelan, M., et al. 2020, MNRAS, 496, 1730
Freitag, M., Amaro-Seoane, P., & Kalogera, V. 2006, ApJ, 649, 91
Gaia Collaboration (Creevey O. L., et al.) 2023, A&A, 674, A39
Galdeano, D., Coldwell, G., Duplancic, F., et al. 2022, A&A, 663, A158
Galdeano, D., Ferrero, G. A., Coldwell, G., et al. 2023, A&A, 669, A7
Garro, E. R., Minniti, D., Gómez, M., et al. 2020, A&A, 642, A19
Garro, E. R., Minniti, D., Gómez, M., et al. 2021a, A&A, 649, A86
Garro, E. R., Minniti, D., Gómez, M., & Alonso-García, J. 2021b, A&A, 654, A23
Garro, E. R., Minniti, D., Gómez, M., et al. 2022, A&A, 658, A120
Garro, E. R., Fernández-Trincado, J. G., Minniti, D., et al. 2023, A&A, 669, A136
Garro, E. R., Minniti, D., Alonso-García, J., et al. 2024, A&A, 688, L3
Gonzalez, O. A., Rejkuba, M., Zoccali, M., et al. 2012, A&A, 543, A13
Gonzalez, O. A., Rejkuba, M., Zoccali, M., et al., 2013, A&A, 552, A110
Gonzalez, O. A., Mucciarelli, A., Origlia, L., et al. 2020, The Messenger, 180, 18
González-Fernández, C., Hodgkin, S. T., Irwin, M. J., et al., 2018, MNRAS, 474, 5459
Graham, M. J., Drake, A. J., Djorgovski, S. G., et al. 2013, MNRAS, 434, 3423
Graham, M., Drake, A., Djorgovski, S. G., Mahabal, A., & Donalek, C. 2017, EPJWC, 152, 03001
Gran, F., Zoccali, M., Contreras, Ramos, R., et al. 2019, A&A, 628, A45
Gran, F., Zoccali, M., Saviane, I., et al. 2022, MNRAS, 509, 4962
Guo, Z., Lucas, P. W., Kurtev, R., et al. 2024, MNRAS, 528, 1769
Herpich, F. R., Ferreira Lopes, C. E., Saito, R. K., et al. 2021, A&A, 647, A169
Irwin, M. J., Lewis, J., Hodgkin, S., et al. 2004, Proc. SPIE, 5493, 411
Ivanov, V. D., Szeifert, & B. Häubler, 2021, VIRCAM/VISTA User Manual, https://eso.org/sci/facilities/paranal/decommissioned/vircam/doc/VIS-MAN-ESO-06000-0002_v108.pdf
Kharchenko, N. V., Piskunov, A. E., Röser, S., et al. 2005, A&A, 438, 1163
Kollmeier, J. A., Zasowski, G., Rix, H.-W., et al. 2017, arXiv e-prints [arXiv:1711.03234]
Kollmeier, J., Anderson, S. F., Blanc, G. A., et al. 2019, BAAS, 51, 274
Lewis, J. R., Irwin, M., & Bunclark, P. 2010, ASP Conf. Ser., 434, 91
Libralato, M., Bellini, A., Bedin, L. R., et al. 2015, MNRAS, 450, 1664
Lomb, N. R. 1976, Ap&SS, 39, 447
Lucas, P. W., Hoare, M. G., Longmore, A., et al. 2008, MNRAS, 391, 136
Lucas, P. W., Smith, L. C., Guo, Z., et al. 2024, MNRAS, 528, 1789
Luna, A., Marchetti, T., Rejkuba, M., & Minniti, D. 2023, A&A, 677, A185
Mainieri, V., Anderson, R. I., Brinchmann, J., et al., 2024, arXiv e-prints [arXiv:2403.05398]
Marchant Cortés, P., Nilo Castellón, J. L., Alonso, M. V., et al. 2024, A&A, 686, A18
Martinez, P., Kolb, J., Sarazin, M., & Tokovinin, A. 2010, The Messenger, 141, 5
McMahon, R. G., Banerji, M., Gonzalez, E., et al. 2013, The Messenger, 154, 35
Meingast, S., Alves, J., Bouy, H., et al. 2023, A&A, 673, A58
Mejías, A., Minniti, D., Alonso-García, J., et al. 2022, A&A, 660, A131
Minniti, D., Lucas, P. W., Emerson, J. P., et al. 2010, New A, 15, 433
Minniti, D., Gómez, M., Alonso-García, J., Saito, R. K., & Garro, E. R. 2021a, A&A, 650, A12
Minniti, D., Palma, T., & Clariá, J. J. 2021b, BAAA, 62, 107
Minniti, D., Matsunaga, N., Fernández-Trincado, J. G., et al. 2024, A&A, 683, A150
Molnar, T. A., Sanders, J. L., Smith, L. C., et al. 2022, MNRAS, 509, 2566
Navarro , M. G., Minniti, D., & Contreras Ramos, R., 2017, ApJ, 851, L13
Navarro, M. G., Minniti, D., & Contreras-Ramos, R. 2018, ApJ, 865, L5
Navarro, M. G., Contreras Ramos, R., Minniti, D., et al. 2020a, ApJ, 893, 65
Navarro, M. G., Minniti, D., Pullen, J., & Ramos R. C. 2020b, ApJ, 889, 56
Obasi, C., Gómez, M., Minniti, D., & Alonso-García, J. 2021, A&A, 654, A39
Obasi, C., Gómez, M., Minniti, D., et al. 2024, MNRAS, 529, 3075
Paladini, R., Zucker, C., Benjamin, R., et al. 2023, arXiv e-prints [arXiv:2307.07642]
Peña Ramírez, K., González-Fernández, C., Chené, A.-N., Ramírez & Alegría, S. 2021, MNRAS, 503, 1864
Peña Ramírez, K., Smith, L. C., Ramírez Alegría, S., et al. 2022, MNRAS, 513, 5799
Rimoldini, L., Holl, B., Gavras, P., et al. 2023, A&A, 674, A14
Saito, R. K., Hempel, M., Minniti, D., et al. 2012, A&A, 537, A107
Saito, R. K., Stecklum, B., Minniti, D., et al. 2023, ApJ, 958, L1
Sanders, J. L., Matsunaga, N., Kawata, D., et al., 2022, MNRAS, 517, 257
Sanders, J. L., Kawata, D., Matsunaga, N., et al. 2024, MNRAS, 530, 2972
Saroon, S., Dias, B., Minniti, D., et al. 2024, A&A, 689, A115
Saviane, I., Zoccali, M., Minniti, D., Geisler, D., & Dias, B. 2020, The Messenger, 179, 31
Scargle, J. D. 1982, ApJ, 263, 835
Schechter, P. L., Mateo, M., & Saha, A. 1993, PASP, 105, 1342
Schlafly, E. F., Green, G. M., Lang, D., et al. 2018, ApJS, 234, 39
Smith, L. C., Lucas, P. W., Kurtev, R., et al. 2018, MNRAS, 474, 1826
Soto, M., Sgró, M. A., Baravalle, L. D., et al. 2022, MNRAS, 513, 2747
Stetson, P. B. 1987, PASP, 99, 191
Surot, F., Valenti, E., Hidalgo, S. L., et al. 2019, A&A, 629, A1
Sutherland, W., Emerson, J., Dalton, G., et al. 2015, A&A, 575, A25
Taylor, M. B. 2006, ASPC, 351, 666
VanderPlas, J. T. 2018, ApJS, 236, 16
Wegg, C., & Gerhard, O. 2013, MNRAS, 435, 1874
Wolf, V., Stecklum, B., Caratti o Garatti, A., et al. 2024, A&A, 688, A8
Zechmeister, M., & Kürster, M. 2009, A&A, 496, 577
Zhang, Y., Zhao, Y., & Wu X.-B. 2021, MNRAS, 503, 5263

[1] Departamento de Física, Universidade Federal de Santa Catarina, Trindade 88040-900, Florianópolis, Brazil
e-mail: roberto.saito@ufsc.br
[2] Instituto de Astrofísica, Dep. de Ciencias Físicas, Facultad de Ciencias Exactas, Universidad Andres Bello, Av. Fernández Concha 700, Santiago, Chile
[3] Max-Planck Institute for Astronomy, Königstuhl 17, 69117 Heidelberg, Germany
[4] Centro de Astronomía (CITEVA), Universidad de Antofagasta, Av. Angamos 601, Antofagasta, Chile
[5] Millennium Institute of Astrophysics (MAS), Nuncio Monseñor Sotero Sanz 100, Of. 104, Providencia, Santiago, Chile
[6] Centre for Astrophysics Research, University of Hertfordshire, College Lane, Hatfield AL1 09A, UK
[7] Vatican Observatory, Specola Vaticana, 00120 Vatican City, Vatican City State
[8] Departamento de Geofísica y Astronomía, CONICET, Facultad de Ciencias Exactas, Físicas y Naturales, Universidad Nacional de San Juan, Av. Ignacio de la Roza 590 (O), J5402DCS, Rivadavia, San Juan, Argentina
[9] Instituto de Astronomía Teórica y Experimental (IATE-CONICET), Laprida 854, X5000BGR, Córdoba, Argentina
[10] Observatorio Astronómico de Córdoba, Universidad Nacional de Córdoba, Laprida 854, X5000BGR, Córdoba, Argentina
[11] Instituto de Física y Astronomía, Universidad de Valparaíso, ave. Gran Bretaña, 1111, Casilla 5030, Valparaíso, Chile
[12] Millennium Institute of Astrophysics, Nuncio Monseñor Sotero Sanz 100, Of. 104, Providencia, Santiago, Chile
[13] Gemini Observatory, Northern Operations Center, 670 A'ohoku Place, Hilo, HI 96720, USA
[14] Wide-Field Astronomy Unit, Institute for Astronomy, University of Edinburgh, Royal Observatory, Blackford Hill, Edinburgh EH9 3HJ, UK
[15] European Southern Observatory, Alonso de Córdova 3107, Casilla 19001, Vitacura, Santiago, Chile
[16] European Southern Observatory, Karl Schwarzschildstr 2, 85748 Garching bei München, Germany
[17] INAF – Osservatorio Astronomico di Capodimonte, Salita Moiariello 16, 80131 Napoli, Italy
[18] Mount Saint Vincent University, Halifax B3M 2J6, Canada
[19] INAF – Osservatorio Astronomico di Roma, Via di Frascati 33, 00078 Monte Porzio Catone, Roma, Italy
[20] Department of Physics and Astronomy, University College London, London WC1E 6BT, UK
[21] Institute of Astronomy, University of Cambridge, Madingley Rd., Cambridge CB3 0HA, UK
[22] Departamento de Física, Universidade Estadual de Feira de Santana (UEFS), Av. Transnordestina, S/N, CEP 44036-900 Feira de Santana, BA, Brazil
[23] Gemini Observatory/NSF's NOIRLab, Casilla 603, La Serena, Chile

[24] Departamento de Astronomía, Universidad de La Serena, Av. Juan Cisternas 1200 Norte, La Serena, Chile
[25] Universidade de São Paulo, IAG, Rua do Matão 1226, Cidade Universitária, São Paulo 05508-090, Brazil
[26] Fundación Chilena de Astronomía, El Vergel 2252, Santiago, Chile
[27] Istituto Nazionale di Astrofisica, Osservatorio Astronomico di Padova, Vicolo dell'Osservatorio 5, Padova 35122, Italy
[28] Space Telescope Science Institute, 3700 San Martin Drive, Baltimore, MD 21218, USA
[29] Department of Physics, University of Wisconsin-Whitewater, 800 West Main Street, Whitewater, WI 53190, USA
[30] Departamento de Astronomia, Instituto de Física, UFRGS, Av. Bento Gonçalves 9500, Porto Alegre, RS, Brazil
[31] Instituto de Ciências Naturais, Humanas e Sociais, Universidade Federal de Mato Grosso, Cidade Jardim, 78550-728 Sinop, Brazil
[32] Vatican Observatory, VORG, Steward Observatory, 933 N. Cherry Avenue, Tucson, AZ, USA
[33] Gerencia De Vinculación Tecnológica, Comisión Nacional de Actividades Espaciales (GVT-CONAE), Falda del Cañete, Córdoba, Argentina
[34] Colégio Militar de Porto Alegre, Ministério da Defesa, Exército Brasileiro, Av. José Bonifácio 363, Porto Alegre 90040-130, RS, Brazil
[35] Instituto de Alta Investigación, Universidad de Tarapacá, Casilla 7D, Arica, Chile
[36] Instituto de Astrofísica,Pontificia Universidad Católica de Chile, Av. Vicuña Mackenna 4860, 7820436 Macul, Santiago, Chile
[37] Centro de Astro-Ingeniería, Pontificia Universidad Católica de Chile, Av. Vicuña Mackenna 4860, 7820436 Macul, Santiago, Chile
[38] Consejo Nacional de Investigaciones Científicas y Técnicas (CONICET), Godoy Cruz 2290, Ciudad Autónoma de Buenos Aires C1425FQB, Argentina
[39] Department of Physics and Astronomy, Seoul National University, Seoul 08826, Republic of Korea, 2 Research Institute of Basic Sciences, Seoul National University, Seoul 08826, Republic of Korea
[40] Departamento de Tecnologías Industriales, Faculty of Engineering, Universidad de Talca, Merced 437, Curicó, Chile
[41] Departamento de Física de la Tierra y Astrofísica & IPARCOS-UCM (Instituto de Física de Partículas y del Cosmos de la UCM), Facultad de Ciencias Físicas, Universidad Complutense de Madrid, 28040 Madrid, Spain
[42] Centro de Astrobiología (CAB), CSIC-INTA, Camino Bajo del Castillo s/n, 28692, Villanueva de la Cañada, Madrid, Spain
[43] Facultad de Matemática, Astronomía, Física y Computación, Universidad Nacional de Córdoba (UNC), Córdoba, Argentina
[44] University of Central Lancashire, Preston, PR1 2HE, UK
[45] Instituto de Ciencias Astronómicas, de la Tierra y del Espacio (ICATE, CONICET), C.C. 467, 5400, San Juan, Argentina
[46] Astronomy Unit, School of Physical and Chemical Sciences, Queen Mary University of London, Mile End Road, London, E1 4NS, UK
[47] Instituto de Astronomía, Universidad Católica del Norte, Av. Angamos 0610, Antofagasta, Chile
[48] Department of Astronomy, Yale University, 219 Prospect Street, New Haven, CT 06511, USA
[49] Instituto de Astronomía y Ciencias Planetarias, Universidad de Atacama, Copayapu 485, Copiapó, Chile
[50] Laboratorio Nacional de Astrofísica LNA/MCTI, 37504-364 Itajubá, MG, Brazil
[51] Centre for Astrophysics and Planetary Science, School of Physics and Astronomy, University of Kent, Canterbury CT2 7NH, UK
[52] Departamento de Astronomia, Casilla 160-C, Universidad de Concepcion, Chile
[53] Instituto Multidisciplinario de Investigación y Postgrado, Universidad de La Serena, Raúl Bitrán 1305, La Serena, Chile
[54] Max-Planck-Institut für Ex. Physik, Giessenbachstrasse, 85748, Garching, Germany
[55] UK Astronomy Technology Centre, Royal Observatory Edinburgh, Blackford Hill, Edinburgh EH9 3HJ, UK
[56] Université Côte d'Azur, Observatoire de la Côte d'Azur, CNRS, Laboratoire Lagrange, Blvd de l'Observatoire, 06304, Nice, France
[57] Centro Internacional Franco Argentino de Ciencias de la Información y de Sistemas (CIFASIS, CONICET–UNR), Rosario, Argentina
[58] Dipartimento di Fisica, Università di Ferrara, Via Giuseppe Saragat 1, Ferrara 44122, Italy
[59] Western Sydney University, Kingswood campus, NSW, Australia
[60] Centro de Astrofísica da Universidade do Porto, Rua das Estrelas, s/n, 4150-762, Porto, Portugal
[61] Miranda House, University of Delhi, India
[62] Inter University centre for Astronomy and Astrophysics, Pune, India
[63] Universidade Federal do Pampa Br 472, Km 585, CP 118 Uruguaiana, RS, Brazil
[64] Department of Physics & Astronomy, Texas Tech University, Box 41051, Lubbock TX 79409-1051, USA
[65] Instituto de Astrofísica de Canarias, Spain
[66] Departamento de Astrofísica, Universidad de La Laguna, Spain
[67] Istituto Nazionale di Astrofisica, Osservatorio di Astrofisica e Scienza dello Spazio di Bologna, Via Gobetti 101, I40129, Bologna, Italy
[68] Department of Astronomy, Graduate School of Science, The University of Tokyo, 7-3-1 Hongo, Bunkyo-ku, Tokyo 113-0033, Japan
[69] Jodrell Bank Centre for Astrophysics, Department of Physics and Astronomy, The University of Manchester, Oxford Road, Manchester M13 9PL, UK
[70] Departamento de Astronomía, Universidad de Chile, Camino El Observatorio 1515, Las Condes, Chile
[71] Association of Universities for Research in Astronomy (AURA), Av. Juan Cisternas 1500, La Serena, Chile
[72] Grupo de Astrofísica Extragaláctica-IANIGLA, CONICET, Universidad Nacional de Cuyo (UNCuyo), Gobierno de Mendoza, Argentina
[73] Department of Physics and Astronomy, Johns Hopkins University, Baltimore MD 21218, USA
[74] Clínica Universidad de los Andes - Dirección Comercial, Av. Plaza 2501, Santiago, Chile
[75] SOAR Telescope/NSF's NOIRLab, Avda Juan Cisternas 1500, 1700000 La Serena, Chile
[76] Centro de Docencia Superior en Ciencias Básicas, Universidad Austral de Chile, Los Pinos s/n, Puerto Montt, Chile
[77] Centre for Basic Space Science, University of Nigeria, 410101 Nsukka, Nigeria
[78] Departamento de Matemática, Universidad de Atacama, Copayapu 485, Copiapó, Chile
[79] NSF NOIRLab/Vera C. Rubin Observatory, Casilla 603, La Serena, Chile
[80] Instituto de Astronomía y Física del Espacio (IAFE, CONICET-UBA), C1428ZAA, Ciudad Autónoma de Buenos Aires, Argentina
[81] Instituto de Estudios Astrofísicos, Facultad de Ingeniería y Ciencias, Universidad Diego Portales, Av. Ejército Libertador 441, Santiago, Chile
[82] Max-Planck-Institut für extraterrestrische Physik, Gießenbachstraße 1, 85748 Garching, Germany
[83] Thüringer Landessternwarte, Sternwarte 5, 07778 Tautenburg, Germany
[84] Department of Physics, University of Warwick, Gibbet Hill Road, Coventry CV4 7AL, UK
[85] Astrobiology Center, 2-21-1 Osawa, Mitaka, Tokyo 181-8588, Japan
[86] National Astronomical Observatory of Japan, 2-21-1 Osawa, Mitaka, Tokyo 181-8588, Japan
[87] Departamento de Física, FACI, Universidad de Tarapacá, Casilla 7D, Arica, Chile
[88] Museo Interactivo de la Astronomía, Centro Interactivo de la Conocimientos, Avenida Punta Arenas 6711, La Granja, Chile
[89] North Optics, Cristóbal Colón # 352 oficina 514, La Serena, Chile
[90] School of Mathematical and Physical Sciences, Macquarie University, Sydney, NSW 2109, Australia

## Appendix A: VVVX tile coordinates and observations

Here we list the tile centre coordinates for all VVV and VVVX pointing. There is a total of 1028 tiles, divided into 348 for the original VVV area and 680 tiles for VVVX. For the original and extended bulge area tiles, names start with 'b'. Inner disk tiles in the original and extended area start with 'd', while for the low and high disk, as well as to disk to longitude +20 names start with 'e'. Fig. A.1 shows the survey area with the tiles positions and respective names. For each tile we provide tile centre coordinates in Equatorial and Galactic systems. All tiles have been observed using an identical offsetting strategy, combining six pawprints to contiguously fill $1.5 \times 1.1$ sq. deg. area. Columns 6, 7 and 8 present the number of epochs taken in $J$, $H$ and $K_s$ during the VVV and VVVX campaigns. The first number is the total of epochs, and in parentheses the number of epochs observed in VVV and VVVX, respectively.

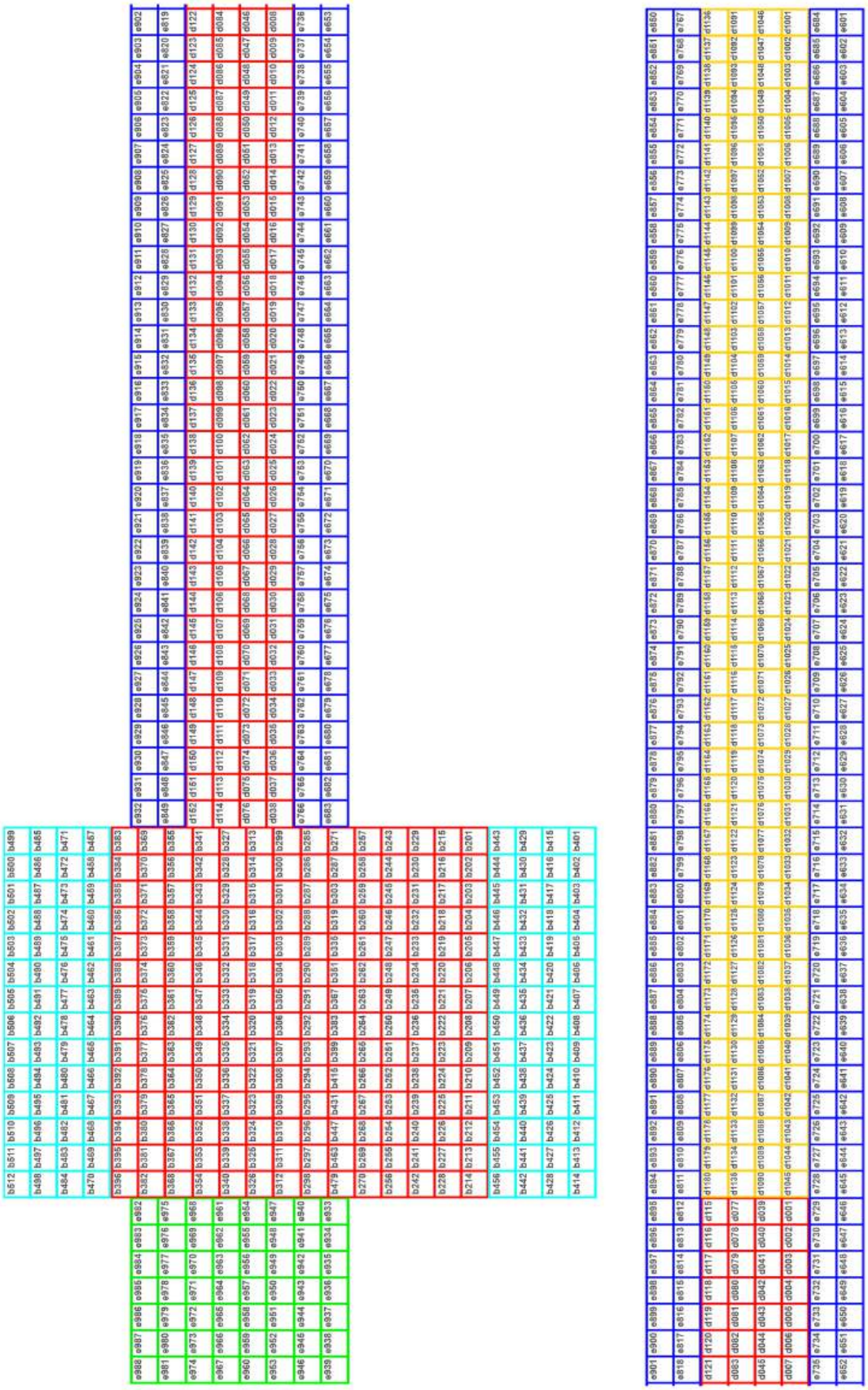

**Fig. A.1.** Zoomed view of the VVVX survey area with the tiles positions and respective names. The original VVV area in shown in red, while the other colours mark the VVVX areas. For the original and extended bulge area tile, names start with 'b'. Inner disk tiles in the original and extended area start with 'd', while for the low and high disk, as well to disk to longitude +20 names start with 'e'.

**Table A.1.** List the VVV+VVVX tiles and observed number of epochs.

| Tile name | RA (J2000.0) (dd:mm:ss.ss) | DEC (J2000.0) (dd:mm:ss.s) | longitude (degrees) | latitude (degrees) | $J$ epochs | $H$ epochs | $K_s$ epochs |
|---|---|---|---|---|---|---|---|
| b0201 | 18:04:36.67 | −41:52:19.1 | −9.344772 | −9.781310 | 2 (2 + 0) | 2 (2 + 0) | 79 (76 + 3) |
| b0202 | 18:08:12.42 | −40:34:54.6 | −7.866743 | −9.781265 | 2 (2 + 0) | 2 (2 + 0) | 80 (76 + 4) |
| b0203 | 18:11:41.75 | −39:17:16.9 | −6.388843 | −9.781293 | 2 (2 + 0) | 2 (2 + 0) | 81 (77 + 4) |
| b0204 | 18:15:05.21 | −37:59:26.7 | −4.910874 | −9.781311 | 2 (2 + 0) | 2 (2 + 0) | 78 (75 + 3) |
| b0205 | 18:18:23.31 | −36:41:25.3 | −3.432812 | −9.781345 | 2 (2 + 0) | 2 (2 + 0) | 78 (75 + 3) |
| b0206 | 18:21:36.47 | −35:23:14.3 | −1.954806 | −9.781319 | 2 (2 + 0) | 2 (2 + 0) | 83 (79 + 4) |
| b0207 | 18:24:45.14 | −34:04:55.1 | −0.476882 | −9.781341 | 2 (2 + 0) | 2 (2 + 0) | 82 (79 + 3) |
| b0208 | 18:27:49.70 | −32:46:28.3 | 1.001059 | −9.781314 | 2 (2 + 0) | 2 (2 + 0) | 80 (76 + 4) |
| b0209 | 18:30:50.53 | −31:27:54.8 | 2.479066 | −9.781278 | 2 (2 + 0) | 2 (2 + 0) | 80 (76 + 4) |
| b0210 | 18:33:47.98 | −30:09:15.9 | 3.957067 | −9.781317 | 2 (2 + 0) | 2 (2 + 0) | 83 (80 + 3) |
| ... | | | | | | | |

**Notes.** Only the first 10 rows of the table are shown here. The full table with the list of the 1028 VVV+VVVX tiles is available in the Zenodo repository through the link https://zenodo.org/records/12587535. We present the tile names and centre coordinates in Equatorial and Galactic systems (see Fig. A.1 for the spatial distribution). Columns 6 to 8 present the number of epochs observed in $J$, $H$ and $K_s$ during the VVV and VVVX campaigns. The first number is the total of epochs, and in parentheses the number of epochs observed in VVV and VVVX, respectively.